Permeability and pressure measurements in Lesser Antilles submarine slides

Hornbach, Matthew J.; Watt, Sebastian

DOI:
10.1002/2015JB012061

Document Version
Publisher's PDF, also known as Version of record

Citation for published version (Harvard):
Hornbach, MJ & Watt, S 2016, 'Permeability and pressure measurements in Lesser Antilles submarine slides: evidence for pressure-driven slow-slip failure', *Journal of Geophysical Research*, vol. 120, no. 12, pp. 7986-8011. https://doi.org/10.1002/2015JB012061

AGU PUBLICATIONS

JGR

Journal of Geophysical Research: Solid Earth

RESEARCH ARTICLE
10.1002/2015JB012061

Key Points:
- Permeability and pressure measurements were made on submarine slide deposits
- Near-lithostatic fluid pressures exist between low-permeability clays in many slide deposits
- Small stress changes can trigger additional shearing and slow-slip failure in some slide sediments

Correspondence to:
M. J. Hornbach,
mhornbach@smu.edu

Citation:
Hornbach, M. J., et al. (2015), Permeability and pressure measurements in Lesser Antilles submarine slides: Evidence for pressure-driven slow-slip failure, *J. Geophys. Res. Solid Earth*, *120*, 7986–8011, doi:10.1002/2015JB012061.

Received 27 MAR 2015
Accepted 7 NOV 2015
Accepted article online 11 NOV 2015
Published online 15 DEC 2015

Permeability and pressure measurements in Lesser Antilles submarine slides: Evidence for pressure-driven slow-slip failure

Matthew J. Hornbach[1], Michael Manga[2], Michael Genecov[1], Robert Valdez[3], Peter Miller[3], Demian Saffer[3], Esther Adelstein[2], Sara Lafuerza[4], Tatsuya Adachi[5], Christoph Breitkreuz[6], Martin Jutzeler[7], Anne Le Friant[8], Osamu Ishizuka[9], Sally Morgan[10], Angela Slagle[11], Peter J. Talling[7], Andrew Fraass[12], Sebastian F. L. Watt[13], Nicole A. Stroncik[14], Mohammed Aljahdali[15], Georges Boudon[8], Akihiko Fujinawa[16], Robert Hatfield[17], Kyoko Kataoka[18], Fukashi Maeno[19], Michael Martinez-Colon[20], Molly McCanta[21], Martin Palmer[22], Adam Stinton[23], K. S. V. Subramanyam[24], Yoshihiko Tamura[25], Benoît Villemant[26], Deborah Wall-Palmer[27], and Fei Wang[28]

[1]Department of Earth Sciences, Southern Methodist University, Dallas, Texas, USA, [2]Department of Earth and Planetary Science, University of California, Berkeley, California, USA, [3]Department of Geosciences, Pennsylvania State University, University Park, Pennsylvania, USA, [4]Institut des Sciences de la Terre, University of Pierre and Marie Curie, Paris, France, [5]Graduate School of Science and Engineering, Yamagata University, Yamagata, Japan, [6]Department of Geology and Paleontology, TU Bergakademie Freiberg, Freiberg, Germany, [7]National Oceanography Centre, Southampton, UK, [8]Institut de Physique du Globe de Paris, Sorbonne Paris Cité, Université Paris Diderot, UMR 7175, CNRS, Paris, France, [9]Geological Survey of Japan, AIST, Tsukuba, Japan, [10]Department of Geology, University of Leicester, Leicester, UK, [11]Lamont-Doherty Earth Observatory, Columbia University, Palisades, New York, USA, [12]Department of Geosciences, University of Massachusetts Amherst, Amherst, Massachusetts, USA, [13]School of Geography, Earth and Environmental Sciences, University of Birmingham, Birmingham, UK, [14]Integrated Ocean Drilling Program, Texas A&M University, College Station, Texas, USA, [15]Earth, Ocean, and Atmospheric Sciences, Florida State University, Tallahassee, Florida, USA, [16]Department of Environmental Sciences, Ibaraki University, Mito, Japan, [17]CEOAS, Oregon State University, Corvallis, Oregon, USA, [18]Research Institute for Natural Hazards and Disaster Recovery, Niigata University, Niigata, Japan, [19]Volcano Research Center, Earthquake Research Institute, University of Tokyo, Tokyo, Japan, [20]College of Marine Science, University of South Florida, St. Petersburg, Florida, USA, [21]Geology Department, Tufts University, Medford, Massachusetts, USA, [22]School of Ocean and Earth Science, University of Southampton, Southampton, UK, [23]Montserrat Volcano Observatory, Flemings, Montserrat Seismic Research Center, University of the West Indies, St. Augustine, Trinidad and Tobago, [24]Geochemistry Division, National Geophysical Research Institute, Hyderabad, India, [25]Institute for Research on Earth Evolution, JAMSTEC, Yokosuka, Japan, [26]Laboratoire de Pétrologie, Géochimie, Volcanologie, Université Pierre-et-Marie-Curie–Paris 6, UMR 7193, ISTEP, Paris, France, [27]School of Geography, Earth and Environmental Sciences, Plymouth University, Plymouth, UK, [28]Institute of Geology and Geophysics, Chinese Academy of Sciences, Beijing, China

Abstract Recent studies hypothesize that some submarine slides fail via pressure-driven slow-slip deformation. To test this hypothesis, this study derives pore pressures in failed and adjacent unfailed deep marine sediments by integrating rock physics models, physical property measurements on recovered sediment core, and wireline logs. Two drill sites (U1394 and U1399) drilled through interpreted slide debris; a third (U1395) drilled into normal marine sediment. Near-hydrostatic fluid pressure exists in sediments at site U1395. In contrast, results at both sites U1394 and U1399 indicate elevated pore fluid pressures in some sediment. We suggest that high pore pressure at the base of a submarine slide deposit at site U1394 results from slide shearing. High pore pressure exists throughout much of site U1399, and Mohr circle analysis suggests that only slight changes in the stress regime will trigger motion. Consolidation tests and permeability measurements indicate moderately low (~10^{-16}–10^{-17} m^2) permeability and overconsolidation in fine-grained slide debris, implying that these sediments act as seals. Three mechanisms, in isolation or in combination, may produce the observed elevated pore fluid pressures at site U1399: (1) rapid sedimentation, (2) lateral fluid flow, and (3) shearing that causes sediments to contract, increasing pore pressure. Our preferred hypothesis is this third mechanism because it explains both elevated fluid pressure and sediment overconsolidation without requiring high sedimentation rates. Our combined analysis of subsurface pore pressures, drilling data, and regional

seismic images indicates that slope failure offshore Martinique is perhaps an ongoing, creep-like process where small stress changes trigger motion.

1. Introduction

Submarine slides are ubiquitous along the flanks of volcanic islands and continental margins. The dynamics of submarine slope failure has important implications for sediment transport, submarine geohazards, and margin evolution [e.g., *Bugge et al*., 1988; *Ward*, 2001; *Masson et al*., 2006; *Gardner*, 2010; *Watt et al*., 2012]. Currently, however, submarine slide dynamics is poorly constrained. Though studies have long-suggested submarine slides fail as rapid, sometimes catastrophic events [e.g., *Kuenen*, 1952; *Hungr*, 1995], more recent studies [*Owen et al*., 1995; *Cervelli et al*., 2002; *Shillington et al*., 2012; *Le Friant et al*., 2015] indicate that submarine slides may also sometimes fail in an incremental, slow-slip, or creep-like manner along overpressured décollement zones. Understanding how submarine slides fail is critically important for assessing submarine geohazards. For example, submarine slide motion (and in particular, slide velocity) has a first-order effect on tsunami generation [e.g., *Ward*, 2001], with rapid (m/s) sliding capable of generating significant waves. In contrast, slow-slip ($<$mm/s) slide deformation, where slide velocity is much lower than the shallow-water wave speed, typically poses no significant tsunami hazard. Multiple studies suggest that elevated pore pressures are a necessary prerequisite to trigger slow-slip landslide failure [e.g., *Hilley et al*., 2004; *Shillington et al*., 2012]. In this study, we test this hypothesis offshore of the Lesser Antilles Islands by calculating the pore fluid pressure in sediments both inside and outside of submarine slide deposits that may experience slow slip [e.g., *Le Friant et al*., 2015]. Our analysis therefore provides insight into whether elevated fluid pressures exist in submarine slide sediments, as previous slow-slip submarine slide studies suggest.

Constraining sediment physical properties and in particular in situ pore fluid pressure provides insight into sediment strength and the possibility of slope failure [e.g., *Stegmann et al*., 2007; *Sawyer et al*., 2009]. Currently, the timing, scale, and dynamics of slope failures along the Lesser Antilles Arc are only moderately constrained [e.g., *Boudon et al*., 2007; *Watt et al*., 2012; *Le Friant et al*., 2015]. Rapid sedimentation can elevate subsurface fluid pressure, promoting slope failure [e.g., *Dugan and Flemings*, 2000; *Schneider et al*., 2009], and recent studies suggest that the largest submarine landslide deposits offshore of Montserrat are complex multistage events in which the rapid deposition of debris avalanche deposits generated excess pore pressure in weaker undrained marine sediments downslope, resulting in progressive failure with relatively little downslope transport [*Watt et al*., 2012, 2014]. *Le Friant et al*. [2015] make similar arguments, and note that the relatively intact, small-offset nature of marine deposits found in submarine slides offshore Montserrat indicates possible slow-slip deformation. If the pressure-driven slow-slip hypothesis is correct, one might anticipate finding elevated fluid pressures in deep marine sediment in submarine slides that facilitate progressive downslope failure. This study derives pore pressures in failed and unfailed deep marine sediments of the Lesser Antilles to test this hypothesis.

Pore pressure can be measured in situ at drill sites using downhole penetrometers [e.g., *Stegmann et al*., 2006, 2007; *Flemings et al*., 2008], logging-while-drilling techniques combined with consolidation tests [e.g., *Moore et al*., 1995; *Moore and Tobin*, 1997; *Saffer*, 2003], and via borehole monitoring [e.g., *Davis et al*., 1992; *Screaton et al*., 1997]. When in situ pressure measurements are not available, they are often estimated using seismic velocities [e.g., *Bangs et al*., 1990; *Dutta*, 2002; *Bowers*, 1995], consolidation tests [e.g., *Moran et al*., 1993; *Morgan and Ask*, 2004; *Spinelli et al*., 2007], or by integrating empirical velocity-porosity-pressure relationships derived via consolidation tests with regional seismic velocity models [e.g., *Carstens and Dypvik*, 1981; *Bowers*, 1995; *Burrus*, 1998; *Eberhart-Phillips et al*., 1989; *Screaton et al*., 2002; *Bangs and Gulick*, 2005; *Tobin and Saffer*, 2009; *Kitajima and Saffer*, 2012]. Each of these methods has advantages and disadvantages. For example, the use of seismic velocity modeling and empirical velocity-porosity-pressure relationships for estimating pressure provides a rapid assessment of in situ pore pressure, but with large uncertainties if there are significant lithologic variations. Consolidation tests provide high-resolution estimates of sediment compaction state, and thus in situ pore pressure, but can only be applied to clay-rich sediment. These measurements also take a significant amount of time and require suitable samples.

Although direct (in situ) pore pressure measurements at Leg 340 drill sites do not exist, we can calculate in situ pressure by integrating Leg 340 physical properties data with rock physics models [*Dvorkin et al*., 1999a; *Mavko et al*., 2009]. We apply this approach because it provides meter-scale depth resolution of pore pressure that

more accurately accounts for sediment lithology compared to typical empirical velocity-porosity-pressure pressure estimates. This approach is capable of detecting a pore fluid pressure ratio (λ^*) in excess of ~0.6 and provides a first-order method for detecting elevated fluid pressures at International Ocean Discovery Program (IODP) sites [*Hornbach and Manga*, 2014]. Here we define the pore fluid pressure ratio (λ^*) as the fluid overpressure divided by hydrostatic effective stress

$$\lambda^* = \frac{P^*}{(\sigma_1 - P_h)} \quad (1)$$

where P^* is the fluid pressure above hydrostatic, σ_1 is the maximum principle stress (assumed vertical), and P_h is the hydrostatic stress. An important advantage of the rock physics model approach for estimating in situ pore pressure versus other empirical approaches or more costly and time consuming in situ pressure measurement methods is its applicability to any environment where lithology is well constrained, grain contact theory holds, and quality downhole seismic velocity logs exist [*Hornbach and Manga*, 2014]. As a result, rock physics models have been applied successfully to a diverse range of lithologies, including clay-rich marine sediments, and are routinely used for pore pressure prediction in oil and gas reservoirs and scientific drill holes [*Helgerud et al*., 1999; *Boyd-Gorst et al*., 2001; *Vanorio et al*., 2003; *Tsuji et al*., 2008].

Here we implement the rock physics approaches of *Dvorkin et al*. [1999a] and *Mavko et al*. [2009] and apply their method throughout entire drill holes where sediment lithology is well constrained. We apply this method to three drill sites, U1394, U1395, and U1399, from IODP Expedition 340 near the Lesser Antilles. U1394 and U1399 were drilled through submarine slide deposits; U1395 was drilled outside all recognized submarine slide deposits [*Leg 340 Scientists*, 2012]. Here we define a submarine slide (and associated slide debris) as cohesive sediment that fails via shearing. In contrast, we define a turbidite as a deposit from a highly dilute sediment-rich fluid that is transported via sediment flow associated with a turbidity current. We recognize turbidites as part of the natural background mechanism for deepwater sediment deposition. At all three sites, logging provides quality in situ wireline *P* wave (V_p) and *S* wave (V_s) seismic velocity measurements [*Leg 340 Scientists*, 2012]. We compare results using the rock physics approach with other geophysical indicators of elevated fluid pressure, including V_p/V_s ratios, porosity-depth values, and other recent pore pressure studies at these sites [e.g., *Lafuerza et al*., 2014]. This analysis is used to test whether significant pore fluid pressure exists in sediments near slide headwalls at site U1394, in more distal slide debris at site U1399, and in unfailed sediment outside known slide events at site U1395.

2. Geologic Background

The Lesser Antilles Arc is an ~800 km long north-south trending chain of volcanic islands located near the eastern terminus of the Caribbean plate (Figure 1). The arc is the manifestation of long-lived (>65 Ma) active subduction of the North and South American plates beneath the Caribbean [e.g., *Macdonald et al*., 2000]. An accretionary wedge and large carbonate platforms reside east of the arc. West of the arc is the Grenada back-arc basin. This basin is bounded by the Lesser Antilles Arc to the east and the Aves Ridge to the west. Having water depths greater than 3000 m, the Grenada basin acts as the primary catchment of sediments eroded from the western flank of the Lesser Antilles Arc.

The submarine environment along the arc and the adjacent Grenada basin provides an ideal location for studying near- and far-field physical properties of mass transport deposits associated with volcanic arcs. Analysis of seismic images combined with shallow sediment cores indicate that the Lesser Antilles experienced geologically frequent and recurrent flank collapses, with most slide debris deposited offshore [e.g., *Le Friant et al*., 2003a, 2003b; *Boudon et al*., 2007; *Lebas et al*., 2011; *Watt et al*., 2012]. During the past 0.1 Ma, at least 13 different volcanoes have erupted along the Lesser Antilles Arc, with activity diminishing approximately symmetrically north and south from the island of Dominica [*Wadge*, 1984; *Lindsay et al*., 2005].

Historic and prehistoric mass transport deposits, including flank collapses and pyroclastic flows, surround the volcanic islands. Analysis of shallow marine cores [*Boudon et al*., 2007; *Le Friant et al*., 2008; *Trofimovs et al*., 2008, 2012, 2013; *Cassidy et al*., 2013] provides insight into mass transport deposits since the late Pleistocene; however, relatively little is known about older, deeper sediments deposited near the Lesser Antilles. Marine geophysical studies, including multibeam and active source seismic surveys along the arc and Grenada basin, reveal several submarine slides that extend from the volcanic islands to perhaps more than 100 km west of the arc into the Grenada basin (Figure 1) [*Le Friant et al*., 2004]. Some of these mass transport deposits, most of

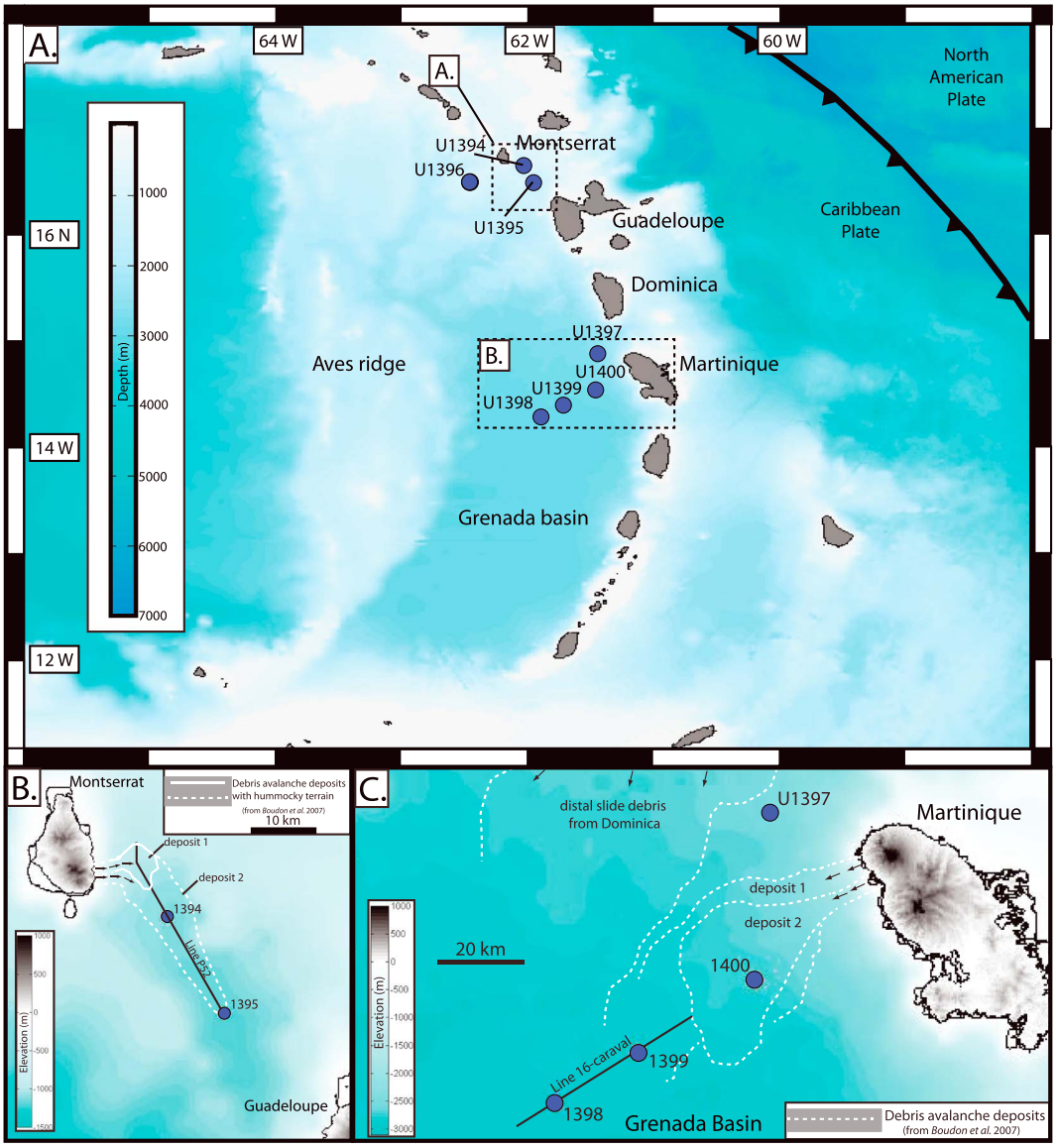

Figure 1. (a) Map showing the location of Leg 340 drill sites (blue dots). (b and c) Dashed boxes in Figure 1a show in greater detail the location of drill sites with respect to mapped slope failure events near Montserrat and Martinique.

which do not exceed 1 km^3, have generated tsunamis or have been inferred to generate tsunamis [*Le Friant et al.*, 2003a, 2003b; *Edmonds and Herd*, 2005; *Boudon et al.*, 2007; *Mattioli et al.*, 2007; *Watt et al.*, 2012].

IODP Leg 340 is the first deep-sea drilling expedition dedicated to scientific drilling of slope failure deposits associated with volcanic island arcs (Figure 2). We focus our study on three IODP Leg 340 drill sites located on the Lesser Antilles Arc and adjacent Grenada basin where R/V *JOIDES Resolution* drilled during the spring of 2012. Site U1394 drilled through slide collapse debris (Deposit 2, Figures 1b and 2a) along the southeast coast of Montserrat [e.g., *Le Friant et al.*, 2009]. Site U1394 is located only ~10 km downslope of the slide headwall. Site U1395 is located ~35 km downslope from the slide headwall and is located just beyond the toe of landslide Deposit 2 (Figure 2a). Site U1394 drilled into "Deposit 2" slide debris, as described by *Boudon et al.* [2007]; however, site U1395 did not drill into any recognized slide deposits. Site U1394 therefore drilled failed material associated with landslide deposits, whereas site U1395 drilled sediments that have not failed. IODP Leg 340 drilled site U1399 in more distal slide debris (>60 km downslope from a slide headwall) in the Grenada basin (Figures 2b and 2c). Slide debris at site U1399 is associated with flank collapse on the island of Martinique (Figure 1c) [*Le Friant et al.*, 2003a, 2003b]. We chose to conduct our analysis at these three drill

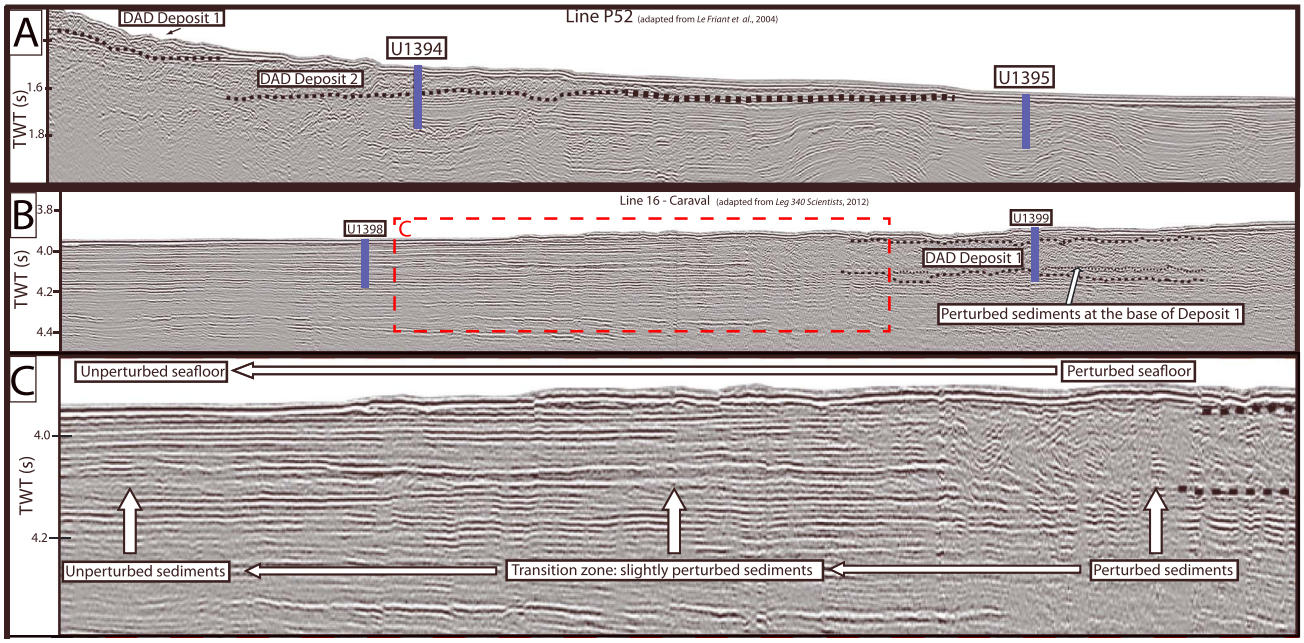

Figure 2. (a) Seismic line P52 shot down the axes of Deposit 1 and Deposit 2 off the southeast coast of Montserrat [*Le Friant et al.*, 2011]. (b) Caraval Line 16 shot approximately east-west over Deposit 1 off the west coast of Martinique [*Le Friant et al.*, 2011]. (c) The red dashed box in Figure 2b is the region shown. The blue lines indicate the approximate location of drill sites. Note in Figures 2b and 2c the seismically chaotic reflection located at depths shallower than ~168 mbsf near site U1399 where we observe the most significant evidence for elevated fluid pressure. Farther to the southwest on Caraval Line 16 (left side of Figure 2c), there is less seafloor and subsurface deformation.

sites because (1) all three sites drilled through sediments either adjacent to or containing slide debris, allowing us to compare physical properties of both failed and unfailed material; (2) they provide different locations to assess potential spatial changes in sediment physical properties of slide debris; and (3) all three sites have the necessary in situ downhole logging V_p and V_s measurements required to determine in situ pore pressure via rock physics modeling. Results are compared with both consolidation tests and V_p/V_s ratios to assess model accuracy.

3. Method: Deriving Pore Pressure From Rock Physics Models

We use the effective-medium rock physics model developed by *Dvorkin et al.* [1999a, 1999b] and *Mavko et al.* [2009] to determine in situ pore fluid pressure with meter-scale vertical resolution. This rock physics model is a first principles approach for calculating in situ seismic velocity and pore pressure. In situ fluid pressures in excess of $\lambda^* > 0.6$ are detectable at IODP sites wherever sediment mineralogy, porosity, and downhole V_p or V_s data exist [*Hornbach and Manga*, 2014]. The rock physics approach uses the bulk and shear moduli for both the saturated and dry sediment frame conditions based on Hertz-Mindlin Contact Theory and Gassmann's equations [*Mindlin*, 1949; *Gassmann*, 1951]. Calculating in situ pore pressure using the rock physics model requires constraining four key parameters: (1) sediment grain elastic moduli, (2) sediment porosity, (3) an average number of particle grain contacts in the sediment, and (4) in situ seismic velocities.

In situ seismic velocities are constrained from analysis of fully processed sonic logs [*Kimball and Marzetta*, 1984]. We determine sediment mineralogy and elastic moduli from detailed (meter- to centimeter-scale) grain size analysis, X-ray diffraction (XRD) analysis, and geochemical analysis of shipboard cores. We constrain in situ porosity measurements from wireline density logs and shipboard measurements. Finally, the number of grain contacts is determined both from theoretical values and empirical studies [e.g., *Smith et al.*, 1929; *Liu and Nagel*, 2010; *Mavko et al.*, 2009].

With constraints (and assigned uncertainties) for each of these variables, we use the rock physics model to calculate in situ seismic velocities at meter-scale resolution assuming hydrostatic conditions. If model-predicted velocities match wireline velocities to within our uncertainty, then we conclude that no evidence

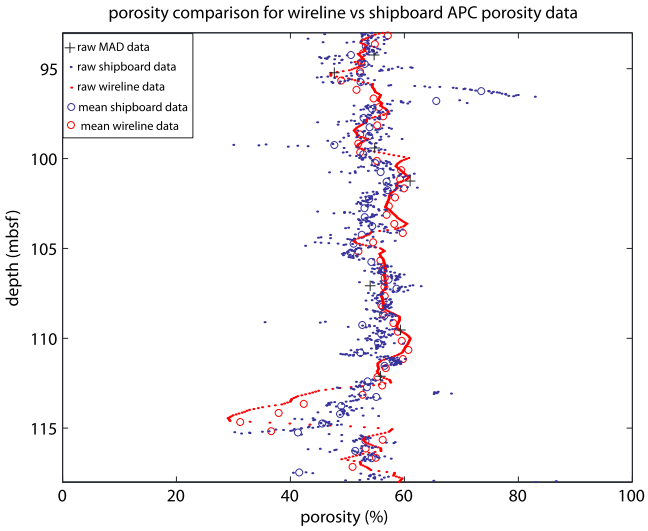

Figure 3. A comparison between in situ and shipboard porosity values. Red values are in situ porosity derived from downhole neutron density logs at hole U1395B; blue values are porosity measurements derived from shipboard neutron density logs. Small points are raw values, and larger open circles are average values over 0.5 m intervals. The depth range shown (93 to 118 mbsl) is the range where wireline neutron density and shipboard neutron density from continuous advance piston core (APC) logs overlap at hole U1395B. Black plus symbols indicate porosity measurements from shipboard MAD data. Using all data available, shipboard-measured porosities are, on average, 0.3% higher than in situ measurements with a standard deviation of ±4.5%, similar with previous porosity studies [e.g., *Hoffman and Tobin*, 2004].

for elevated fluid pressure exists. If, however, modeled velocities fail to match in situ conditions beyond our uncertainty, we adjust the pore pressure in the model to determine the value that provides the best match between modeled and measured in situ seismic velocity.

Pore pressure is not the only significant cause of seismic velocity changes. As already noted, several other factors, including porosity, grain contact number, and mineral changes all impact in situ velocity. Here we describe how we use Leg 340 downhole and shipboard measurements to estimate porosity, grain contact number, and mineralogy values and their associated uncertainty.

3.1. Constraining Porosity

At site U1395, in situ porosity measurements are derived from neutron density logging data. To calculate porosity (φ) from the neutron density (ρ_n), we assume an average grain density (ρ_d) of 2700 kg/m^3 and seawater density (ρ_w) of 1028 kg/m^3, consistent with measured shipboard values derived from moisture and density measurements made on samples [*Leg 340 Scientists*, 2012]. In situ porosity is calculated using the following equation:

$$\varphi = \frac{\rho_n - \rho_d}{\rho_w - \rho_d}. \tag{2}$$

Although we used the neutron density log to determine in situ porosity at site U1395, we also obtained porosity values shipboard via neutron density measurements made on core in the ship's lab and from direct measurements of porosity on discrete core samples from moisture and density measurements [*Leg 340 Scientists*, 2012]. Comparing shipboard versus in situ porosity measurements provides insight into porosity uncertainty at each site. We compare in situ porosity measurements with shipboard porosity measurements at drill hole U1395B from depths between ~93 and ~118 meters below seafloor (mbsf); this depth range is where both wireline neutron density data and continuous advanced piston core (APC) recovery overlap (Figure 3). The sampling interval for shipboard neutron density measurements (5 cm) is different than the in situ neutron density sampling interval (5.1 cm), and correlation of shipboard and wireline logs suggests a depth uncertainty of approximately 0.5 m between the logs. To account for both differences in sampling interval and depth uncertainty, we calculate the average density and porosity for each of the logs at 0.5 m intervals and compare these average values to each other. Comparison between in situ and shipboard porosity estimates at site U1395 suggests an average difference of 0.4% with a standard deviation between shipboard and in situ porosity measurements averaging ±4.5%. The calculated porosity uncertainty between in situ and shipboard measurements of a few percent is consistent with previous studies comparing shipboard and in situ porosities [e.g., *Leg 190 Shipboard Scientific Party*, 2001; *Hoffman and Tobin*, 2004].

To further test the accuracy of this approach, and the approach of using neutron density as a means of estimating porosity, we compare direct measurements of shipboard porosity to wireline neutron density (Figure 3). During the expedition, leg 340 scientists routinely measured porosity every few meters of core with a pycnometer. The pycnometer porosity measurements are included as part of the standard suite of moisture and density data (MAD) collected shipboard by physical properties scientists. For our analysis, we

Table 1. Physical Property Values Used in the Rock Physics Model

Mineral	Grain Density (kg/m^3)	Bulk Modulus (GPa)	Shear Modulus (GPa)
Ryolite	2600	39.5	26.5
Andesite	2700	50	32.5
Basalt	2800	67	36.5
Calcite	2700	76.8	32
Clay	2700	20.9	7
Seawater	1028	2.3	0

compared MAD porosity measurements collected over the same depth range as site U1395 neutron porosity logs (~93–118 mbsf). Although only eight MAD samples exist for this depth range, MAD porosity values mimic measured downhole neutron porosities, with MAD porosity values, on average, 1.3% (±2.7%) higher than wireline neutron porosity values, perhaps because sediment is disturbed during sampling. The analysis, although limited, suggests uncertainties of a few percent in porosity determined from either wireline logs or shipboard data.

As a conservative approach, we assume an uncertainty for porosity values of ±4.5%, the maximum 1 sigma uncertainty we measure between different porosity measurement techniques. In addition, the rock physics analysis ignores any log data where porosity values either exceed 75% or are below 25%, as these values are likely spurious [e.g., *Hamilton*, 1976].

3.2. Constraining Leg 340 Sediment Mineralogy and Sand-to-Mud Ratios

General knowledge of the clay-to-sand ratio in the sediment matrix is important to accurately develop a rock physics velocity model since the velocities of shallowly buried marine sediment consisting of 100% hemipelagic clay or 100% quartz-rich sand differ by approximately 10% for V_p and nearly 50% for V_s [*Hornbach and Manga*, 2014]. We constrain sediment mineralogy and, from this, elastic moduli, using detailed core descriptions painstakingly assembled for each drill site by shipboard scientists on Leg 340 that are cross checked with X-ray diffraction (XRD) analysis using the program *RockJock11* [*Eberl*, 2003]. The core descriptions provide as high as centimeter-scale resolution of basic mineralogy and average grain size defined using the international organization for standardization (ISO) phi scale at each hole where leg 340 scientists obtained cores. In some instances, these average grain size measurements are approximate because the sediment is a mixture of many sizes, and smaller grain sizes (especially below 150 μm) are difficult to estimate by eye. Shipboard scientists digitized basic mineralogy and grain size values for easy import into the rock physics model. XRD analysis has lower spatial resolution than core descriptions, with XRD samples analyzed only every 5–10 m. An additional problem with XRD analysis is that data were most frequently analyzed in the first centimeter of section 1 for each core—a zone typically filled with sediment debris associated with borehole wall collapse [*Jutzeler et al.*, 2014]. As a result, useful XRD data that accurately depict in situ mineralogy generally exist only at depth intervals of 10 m or more where samples from deeper core sections exist.

We broadly define sediment mineralogy and associated elastic moduli at Leg 340 sites by assigning relative bulk quantities for clay, volcaniclastic sand, and calcium carbonate at 0.1 to 5 m intervals in the core. We assign appropriate elastic moduli for the estimated mineralogy with depth using a weighted average that accounts for different mineral ratios found at each depth interval (Table 1). Shipboard stratigraphic analysis shows a clear correlation between sediment grain size and hemipelagic clay content, with finer-grained sediment typically containing more clay [*Leg 340 Scientists*, 2012]. We assign all sediments with shipboard average grain size ISO phi values of 5, 4, and 3 clay percentages of 95%, 68%, and 10%, respectively, based directly on shipboard observations with an estimated uncertainty of ±10% for each [*Leg 340 Scientists*, 2012]. For sediment with phi values less than 3 (i.e., fine-grained sand or larger), clay content is most likely zero but, accounting for uncertainty, clay content may be as high as 10%.

Clear consistency exists between XRD-predicted mineralogy and the texture and composition predicted via core description and shipboard grain size analysis. XRD analysis consistently predicts higher clay content in regions where core description and grain size analysis indicate higher clay content; however, absolute estimates for clay sometimes differ by 10–20%, with XRD analysis typically indicating lower clay content than core descriptions in finer-grained sediment (Table 2). Bias in XRD measurements often exceeds 10% [*Eberl*, 2003]; likewise, we attribute a 10% uncertainty in clay content for a given grain size using core description

Table 2. Clay Content Comparison, Phi Versus XRD Analysis, Site U1399

Depth (m)	Site/Core/Section/Interval	Max Phi Measured	Phi-Estimated Clay %	XRD-Estimated Clay %
1.59	U1399A, 1H, 2, 0–1 cm	1.00	0–10%	13%
94.29	U1399A, 12H, 3, 0–1 cm	1.00	0–10%	12%
126.4	U1399A, 16H, 4, 0–1 cm	6.00	85–100%	36%
158.29	U1399A, 20H, 4, 0–1 cm	4.00	58–78%	40%
175.78	U1399A, 24H, 3, 100–101 cm	3.00	0–20%	25%

methods. As a result, much, if not all of the 10–20% difference between XRD and core description-based mineralogy can be accounted for via these biases. In general, XRD estimates for clay content closely match values based on grain size analysis when sediments are sand-rich and grains are large but XRD predicts significantly lower clay content (~20% less) where fine-grained sediment exists. If the XRD analysis is accurate, it implies that our approach using grain size analysis as a tool for estimating clay content likely underpredicts sand content in fine-grained sediment and that our approach will underpredict in situ velocity and in situ pore pressure in finer-grained sediment [*Hornbach and Manga*, 2014]. The grain size approach is used to estimate clay content because it is a more conservative approach to estimate pore pressure, since higher clay content results in lower velocities and lower in situ pore pressure estimates. XRD analysis, observed clay swelling at each drill site, and other regional XRD studies [*Buatier et al*., 1992; *Brown et al*., 2001] support the premise that the clay encountered at Leg 340 drill sites consists primarily of smectite. As a first-order approach, we therefore assume smectite as the predominate clay mineral.

For the sandy component of the sediment matrix, the elastic moduli of the sand depend on the mineralogy of the sand grains. Sandy sediments found near the Lesser Antilles are generally andesitic, but rhyolitic, basaltic, and bioclastic carbonate sands also exist, with sometimes significant variability in mineralogy [*Brown et al*., 1977; *Smith et al*., 1980; *Baker*, 1984; *Devine*, 1995]. Basalt has the highest elastic moduli of volcaniclastic sediments, and rhyolite has the lowest; the elastic moduli of andesite fall between basalt and rhyolite values [*Malfait et al*., 2011] (Table 1). Knowing the precise mineralogy of volcaniclastic sediment with centimeter-scale resolution in each core is difficult; however, elastic moduli values for basalt, rhyolite, and andesite can be used as a means to estimate maximum, minimum, and average values, respectively, for the volcaniclastic sand grain elastic moduli. By using each of these mineralogy values for the elastic moduli of sands, we see the effect of different sediment grain mineralogy on rock physics model results. Our analysis demonstrates that variations in sand mineralogy between the minimum and maximum end-member values (i.e., 100% rhyolite to 100% basalt) change seismic velocities at Leg 340 drill sites by no more than 2% for V_p and ~10% for V_s. Relative mud-to-sand ratios are likely a factor of 5 more important than the precise sand grain mineralogy [*Hornbach and Manga*, 2014]. Nonetheless, possible uncertainties associated with mineralogy are accounted for by using both rhyolite and basalt as end-member compositions in the model.

In addition to mud and volcaniclastic sand concentrations, we also determined the amount of calcium carbonate using a Coulometrics 5011 CO_2 coulometer. During the cruise, Leg 340 shipboard geochemists measured calcium carbonate concentrations with the coulometer by sampling cores, on average, every 5 m at a site. These measurements provide percent weight values for the amount of calcite found at each sample location with instrument uncertainties of ±1%. The small uncertainty (±1%) in calcium carbonate measurements generates only a tiny change (generally ≪1%) in rock physics model velocity results, and we therefore neglect this uncertainty [e.g., *Henriet et al*., 2005]. With porosity, sediment density, and pore water density also constrained by measurements, we converted weight percent of calcium carbonate into bulk percent calcite for each measurement. Calcium carbonate is sampled at lower spatial resolution (~5 m) than sediment grain measurements. To make use of the high-resolution sediment grain measurements, we therefore linearly interpolate calcium carbonate measurements between sample sites but acknowledge that significant variability in calcium carbonate may exist between samples. Shipboard geochemists also measured the amount of organic carbon found in sediment samples. These measurements indicate that organic carbon concentrations are low (typically less than 1%) and are therefore neglected in the rock physics model.

3.3. Constraining the Number of Grain Contacts

The number of contacts between grains also influences rock physics model results. If sediment grains are loosely packed and therefore have few grain contacts, they move relatively freely when stressed and behave

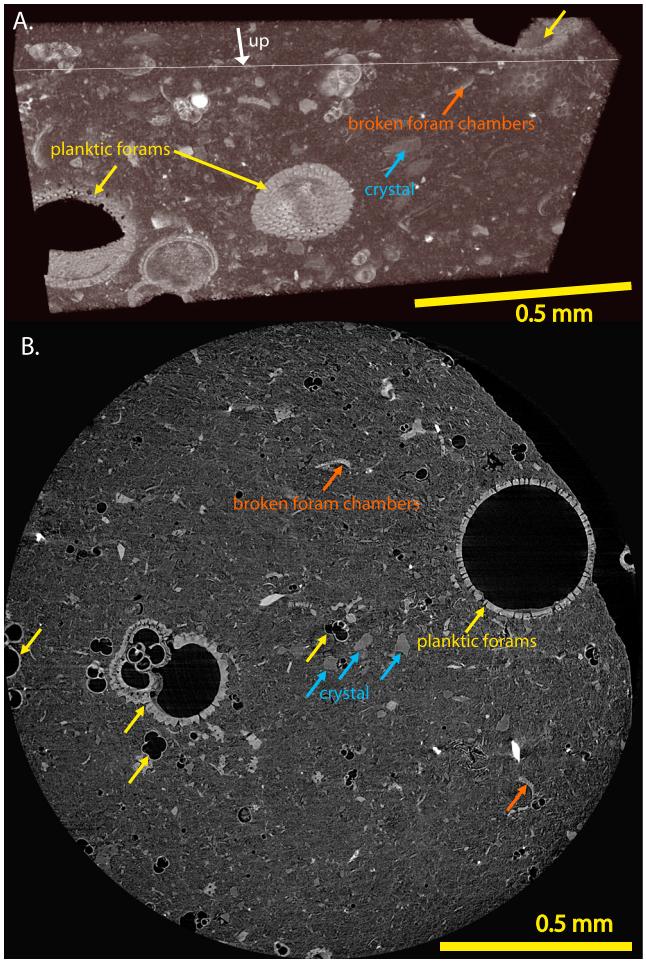

Figure 4. X-ray tomographic images of hemipelagic mud within site U1399 obtained at a depth of ~137 mbsf (0.32 m below the top of core U1399B-19H3). The image is of a cylindrical sediment sample that has a diameter of 1.5 mm and length of 0.37 mm. (a) A 3-D perspective of sediment grains in the X-ray image. (b) A slice through the 3-D image, approximately perpendicular to vertical. The sediment matrix consists of both fully intact (yellow arrows) and broken (orange arrows) microfossils, as well as mineral grains (blue arrows). We observe no obvious fabric in the sediment. Each cubic voxel has a side length of 0.65 μm. Images were created via synchrotron-sourced hard X-ray microtomography at the Advanced Light Source, Lawrence Berkeley National Lab. Energy: 18 keV; camera: PCO.edge sCMOS; exposure: 2049 images at 300 ms with 40 dark fields; Octopus software (www.inct.be/en/software/octopus) for tomographic reconstruction and ImageJ for visualization (Fiji.sc). The image is a map of density, with black low and white high. Porosity inside the foraminifera makes up ~5% of the total volume. How the breakup of foraminifera contributes to pore pressure with time remains unclear but represents perhaps an interesting topic of research.

like a fluid, exhibiting no significant shear. If particles are packed tightly, however, they cannot move freely and behave like a solid [e.g., *Liu and Nagel*, 2010]. In general, tighter grain packing results in more grain contacts, higher elastic moduli, and higher V_p [*Mindlin*, 1949; *Dvorkin et al.*, 1999a; *Liu and Nagel*, 2010].

Determining the number of grain contacts directly is difficult. Detailed 3-D X-ray tomographic (XRT) images of marine sediments collected ~137 mbsf at site U1399 reveal the complexity of grain contacts at the micrometer scale (Figure 4). To the eye, these sediments appear to consist primarily of homogenous, hemipelagic mud. The XRT images clearly demonstrate the complexity and nonuniformity of grain size, shape, and contacts within the mud at the micrometer scale. It also demonstrates how intact versus broken microfossils may impact porosity. Both fully intact and broken microfossils represent the largest structures in the sediment matrix. Our analysis indicates ~5% of the total volume is pore space inside unbroken microfossils. If these microfossils remain intact and matrix porosity is only ~25%, as much as ~20% of the pore space is therefore not accessible to compaction. Why some microfossils compact and others do not is unclear. Even with 3-D XRT images with resolution of 0.6 μm per pixel, accurately constraining the number of grain contacts throughout the section was not possible. We therefore use grain contact values derived from both theoretical and experimental work for our model, as this approach has been shown in the past to accurately represent in situ rock physics properties at mud-rich sites [*Helgerud et al.*, 1999; *Hornbach and Manga*, 2014].

For grains consisting of identical spheres, the minimum number of grain contacts necessary for sediment to behave like a solid is 6, with a greater number of grain contacts increasing the rigidity of the sediments, resulting in higher seismic velocities [e.g., *Liu and Nagel*, 2010, and references therein]. Increased effective stress or frequent shaking from earthquakes increases the number of grain contacts such that the total number of grain contacts can in some extreme instances be as high as 12 [*Mavko et al.*, 2009]. We can constrain the number of grain contacts using experimentally derived relationships between porosity and measured grain contact number. Lower porosities result in a higher number of grain contacts [*Smith et al.*, 1929;

Table 3. Parameters Used for Best Estimate and End-Member Rock Physics Velocity Models

Model Type	Mean # of Grain Contacts	Porosity	Sand Grain Mineralogy	% Clay Content for Phi ≥ 5	% Clay Content for Phi = 4	% Clay Content for Phi = 3	% Clay Content for Phi < 3
Best estimate velocity	7.5	Measured value	Andesite	95%	68%	10%	0
Minimum end-member velocity	6	Measured value +4.5%	Rhyolite	100%	78%	20%	10%
Maximum end-member velocity	9	Measured value −4.5%	Basalt	85%	58%	0%	0%

Manegold and von Engelhardt, 1933; *Murphy*, 1982; *Mavko et al*., 2009]. Porosity values for Leg 340 drill sites typically range between 65% and 35%. These porosity values are consistent with grain contact numbers ranging between 6 and 9, based on experiments using both packed identical [*Smith et al*., 1929; *Manegold and von Engelhardt*, 1933] and nonidentical spheres [*Murphy*, 1982]. Although grains are never perfectly spherical, this first-order assumption for grain shape has proven effective for estimating in situ velocities in marine sediments, including clay-rich sediment [e.g., *Helgerud et al*., 1999; *Mavko et al*., 2009]. This is likely because the number of grain contacts have a relatively small impact on in situ velocity, with contact values between 6 and 9 changing model-predicted V_p and V_s values by a maximum of 3.3% for V_p and a maximum of 12.7% for V_s for most shallow marine sediment [*Hornbach and Manga*, 2014]. The rock physics model analysis therefore indicates that a 50% increase in the number of grain contacts has a relatively minor effect on seismic velocities compared to other uncertainties such as grain mineralogy and porosity. Based on measured porosity values at Leg 340 Sites, we assume grain contact numbers range between 6 and 9 for our rock physics model.

3.4. Generating End-Member Model Uncertainties Values

To determine whether discrepancies between model-predicted seismic velocities and measured in situ velocities are real, we must account for all rock physics model uncertainties. To generate model results, we first calculate the most probable velocity value based directly on the measured physical properties. We then use our uncertainty values for each of the physical properties input in the model to calculate end-member maximum and minimum velocity values at each depth location.

For our best estimate of modeled in situ velocities, we assume that (1) derived porosity values from the logs are correct, (2) the mean number of grain contacts is 7.5, (3) all sand grains consist of 100% andesite, and (4) sediments with grain size ISO phi values of 5, 4, and 3 have clay percentages of 95%, 68%, and 10%, respectively (Table 3). To calculate minimum end-member in situ velocities, we assume that (1) all measured porosity values are too low by 4.5%, (2) the mean number of grain contacts is the theoretical minimum of 6, (3) all sand grains consist of 100% rhyolite, and (4) sediments with grain size ISO phi values of 5, 4, and 3 have clay percentages of 100%, 78%, and 20%, respectively (Table 3). Finally, to calculate maximum end-member in situ velocities, we assume that (1) derived porosity values from the logs are too high by 4.5%, (2) the mean number of grain contacts is 9, (3) all sand grains consist of 100% basalt, and (4) sediments with grain size ISO phi values of 5, 4, and 3 have clay percentages of 85%, 58%, and 0%, respectively (Table 3). Each of these calculations is performed at 0.1 m intervals at sites U1394, U1395, and U1399 where data exist. Due to low spatial sampling of calcium carbonate measurements and hole correlation differences [*Leg 340 Scientists*, 2012], we smooth rock physics model velocity results over a 5 m interval using a running average.

4. Results

Model-predicted seismic velocities, assuming hydrostatic pressure, generally increase with depth, consistent with in situ measurements at all three drill sites. Best estimate hydrostatic rock physics model velocities at site U1394 accurately predict in situ seismic velocities at most depths. The one exception at site U1394 occurs at a depth of ~100 m, where the rock physics model V_s values overpredict observed seismic velocities (by as much as 80% for V_s) (Figure 5a). Best estimate hydrostatic rock physics modeled velocities at site U1395 are consistent with or slightly overpredict observed in situ seismic velocities (Figure 5b). Best estimate hydrostatic rock physics model velocities at site U1399 generally match or slightly overpredict observed in situ seismic velocities, with sometimes significant differences between model-predicted and observed velocities throughout (Figure 5c). The discrepancies between observed and modeled seismic velocities at site U1399 are the most significant and widespread of the three sites studied, with differences greater than 100 m/s in V_s at several depth intervals, and discrepancies that extend well beyond our end-member uncertainty (Figure 6).

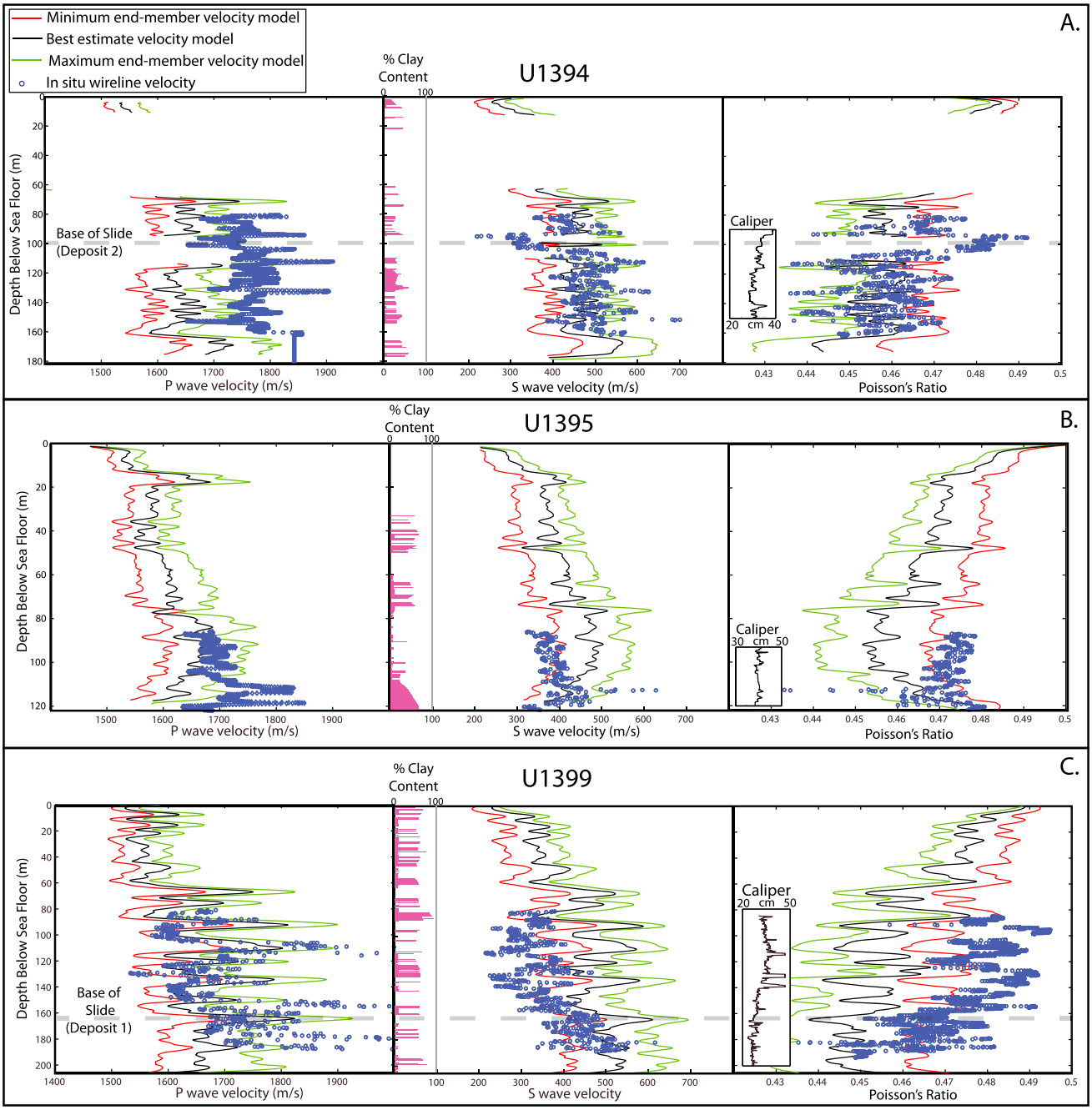

Figure 5. Modeling results for V_p, V_s, and Poisson's ratio at sites U1394, U1395, and U1399. Red lines represent minimum end-member velocity estimates where sand grains are rhyolite, porosity is 4.5% greater than measured values, the number of grain contacts is 6, and clay content is weighted toward the maximum estimate. Black lines represent our best estimate for velocity, where sand grains are andesite, porosity equals our measured value, the number of grain contacts averages 7.5, and clay content is our mean measured value. Green lines represent maximum end-member velocity estimates, where sand grains are basalt, porosity is 4.5% less than the measured values, the number of grain contacts averages 9, and clay content is weighted toward the minimum estimate. Blue dots are actual in situ velocity and Poisson's ratio values measured from wireline logging. Pink bars show the measured amount of clay content with depth at each site. Caliper logs indicate that high-quality hole conditions exist at all three sites. Only U1399 has three limited (meter-scale) zones where hole conditions deteriorate and widen to the maximum possible width. Note that lower velocities generally correlate with higher clay content. In general, results for sites U1394 and U1395 match in situ values. At site U1399, however, inconsistencies between modeled and observed seismic velocities and Poisson's ratio exist at several depth intervals.

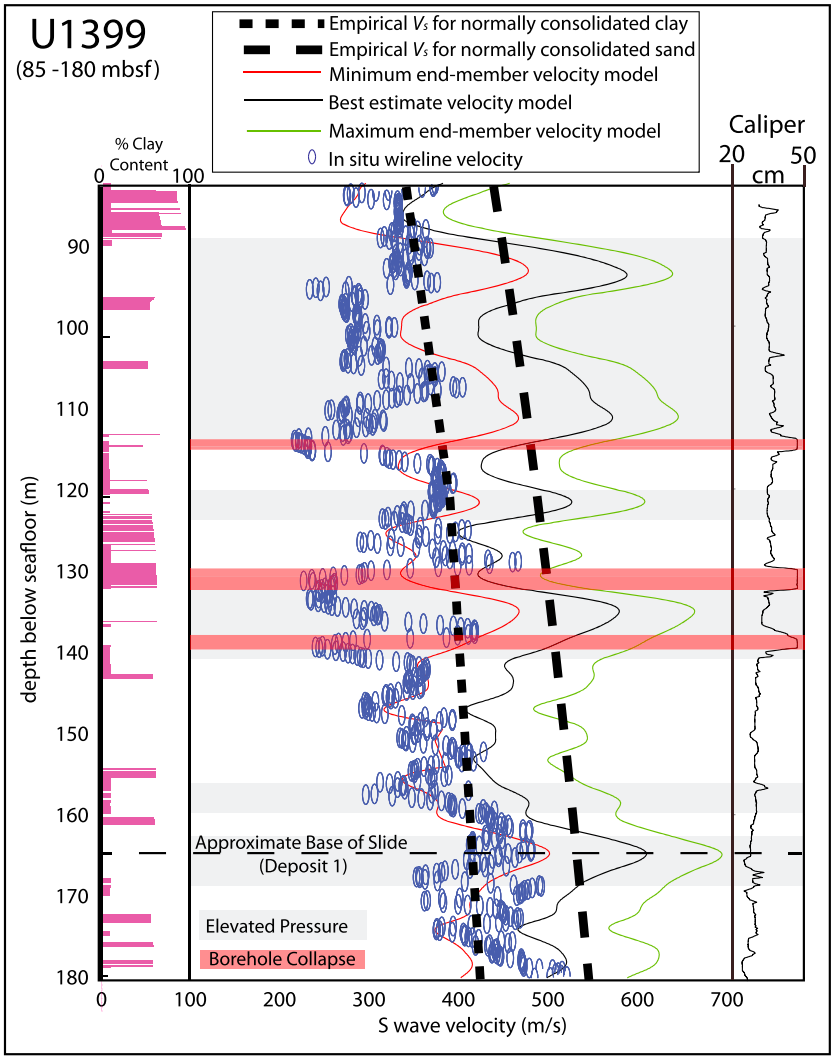

Figure 6. A detailed view of site U1399 V_S results. Gray zones indicate depth regions where there are clear discrepancies between modeled in situ velocities and measured in situ velocities, with measured values consistently too low. The gray zones are areas where elevated fluid pressures are inferred. The potentially overpressured zones generally appear to be sand-rich bodies bounded by clay-rich sediments, as indicated by the pink bars on the left showing where higher clay content exists. Near-vertical black dashed lines show empirical estimates for V_S versus depth for normally consolidated marine sediments based on *Hamilton* [1979]. In situ measurements of V_S are systematically lower than both rock physics model predictions and empirical estimates at several depth intervals. The caliper log indicates that high-quality hole conditions exist at most—but not all—zones where anomalously low in situ seismic velocities exist, implying that our interpretation of high pore pressure zones at site U1399 is likely robust at several depth intervals.

At site U1394, wireline velocity logs extend from approximately 80 to 170 mbsf with V_S and V_P typically ranging between 400 and 700 m/s and 1600 and 1900 m/s, respectively. For this depth range, model predicted in situ V_S velocities generally mimic measured V_S in situ values (Figure 5a) and model-predicted V_P values generally underpredict observed in situ velocities. A best fit for V_S occurs when either andesitic/basaltic sand grains exist, or if the model slightly underestimates mean porosity by 2–3%. The one clear discrepancy between the model predictions and observed in situ velocities occurs at depths of ~100 m, where the model-predicted V_S values are more than 100 m/s higher than observed. This depth interval is consistent with the observed depth for the base of the slide (known as Deposit 2) at Site U1394 (Figure 2a).

At Site U1395, wireline velocity logs overlap continuously with the APC logs from approximately 90 to 120 meters below sea level (mbsl). V_S and V_P values for this depth interval typically range between 300 and 500 m/s and 1640 and 1850 m/s, respectively. Model-predicted in situ velocities generally match measured

in situ V_p and V_s velocities at this site (Figure 5b). A best fit occurs when rhyolitic-to-andesitic sand grains are assumed. At some depths, model-predicted V_s values slightly overpredict observations, but not significantly beyond end-member uncertainties.

At site U1399, wireline velocity logs overlap with continuous APC coring from approximately 85 to 200 mbsf. Both measured and modeled V_s and V_p values for this site have the greatest variability, ranging between 200 and 550 m/s for V_s and 1500 and 2000 m/s for V_p. At depths shallower than ~168 mbsf at this site, a poor fit generally exists between modeled and measured in situ velocities, especially for V_s, with the measured in situ V_s velocity generally lower than modeled V_s velocity values. At site U1399 the modeled minimum end-member velocity estimate fails to overlap the lowest measured in situ velocities at several depth intervals (Figure 6). For example, we observe what appears to be a nearly continuous zone of anomalously low wireline velocities compared to model predictions at depths between ~130–140 mbsf and 90–115 mbsf that is especially well pronounced in V_s data. In these zones, V_s measurements are generally 100 to 200 m/s slower than end-member minimum velocity predictions (Figure 6). Similar discrepancies exist for V_p velocities in some of these depth ranges as well. We identify at least five depth intervals with thicknesses greater than 3 m where significant ($>$50 m/s in V_s) discrepancies between modeled end-member velocities and observed in situ seismic velocities exist, with the most significant ($>$100 m/s in V_s) discrepancies existing between depth intervals of 130–140 mbsf and 90–115 mbsf. The sediments at the depth intervals where velocity discrepancies occur at site U1399 primarily consist of sand-rich deposits bounded by clay-rich layers (Figure 6). The depth where the highest velocity discrepancies exist typically occurs at locations where we see chaotic seismic reflections associated with slide deposits offshore Martinique (Figure 2).

5. Interpretation of Measured Wave Speeds

5.1. The Cause of Anomalously Low In Situ Velocities at 95–105 mbsf at Site U1394

In situ seismic velocities at site U1394 generally fall between end-member model velocity estimates with the exception of the interval from 95 to 105 mbsf. At these depths, the model-predicted velocities for V_s overestimate observed in situ velocities by as much as 200 m/s. Since the model accounts for large uncertainties in porosity, grain contact, grain size, and mineralogy, we suggest that the anomalously low velocities observed in this depth interval are a result of elevated pore fluid pressure. The depth interval where elevated pore fluid pressure exists at U1394 coincides with the approximate base of slide Deposit 2 offshore Montserrat (Figure 2a) and also coincides with a sand-rich zone littered with mud-rich, low bulk density clasts that are chaotically distributed at this depth interval in the core [*Leg 340 Scientists*, 2012]. It is well documented that shearing will reduce sediment permeability, resulting in less fluid flow across a shear zone [e.g., *Bjerrum*, 1967; *Palmer and Rice*, 1973; *Yeo et al*., 1998; *Crawford et al*., 2008], and we therefore suggest that shearing at the base of the slide may have created a low-permeability seal that reduces fluid flow across the interface, resulting in elevated fluid pressure in the shear zone.

Outside the 95–105 mbsf depth interval, modeled velocities are typically slightly below values observed in situ (although all values are within uncertainty). Lower in situ porosities and overconsolidation at this site provides the simplest explanation for our best estimate rock physics model slightly underpredicting observed seismic velocities. Overconsolidation at this site is consistent with previous interpretations that suggest significant erosion due to frequent slope failure [e.g., *Le Friant et al*., 2003a, 2003b; *Boudon et al*., 2007; *Underwood et al*., 2005]. Modeled Poisson's ratio values at site U1394 also closely match measured in situ values at all depths outside 95–105 mbsf. This analysis therefore implies that high pore pressures ($\lambda^* > 0.6$) exist at the base of the slide deposit at a depth of 95–105 mbsf, but no significant elevated fluid pressures likely exist in other sediments drilled at site U1394.

The elevated fluid pressure found at the base of slide Deposit 2 may in part be the result of recent sediment loading on the low-permeability shear zone at the base of Deposit 2. Slide Deposit 2 emplaced volcanic material on the seafloor at ~130 ka [*Watt et al*., 2012; *Le Friant et al*., 2015]. Fluid pressure would have increased below slide Deposit 2 when a second large debris avalanche (termed Deposit 1) was deposited on the seafloor at 12–14 ka just upslope of slide Deposit 2 [e.g., *Watt et al*., 2012], since rapid loading would increase overburden on the low-permeability seal. The results of our study suggest that the second debris avalanche (Deposit 1) may have therefore been emplaced on already overconsolidated sediment

(Deposit 2) that had a low-permeability seal at its base. This loading elevated fluid pressure at the base of Deposit 2 but may not have necessarily triggered failure. Future permeability tests and numerical modeling of pore pressure evolution during loading at this site will provide insight into the role of recent slides at Montserrat on fluid pressure at the base of Deposit 2.

5.2. Analysis of Site U1395 Model Results

Modeled seismic velocities at site U1395 generally match measured in situ seismic velocities. Modeled best estimates for V_s at site U1395 slightly overpredict in situ measurements, whereas modeled best estimates for V_p at site U1395 slightly underpredict measured in situ V_p. In both cases, however, measured in situ velocity values generally fall within a few tens of m/s of end-member uncertainties. The analysis therefore indicates no significant overpressure at this site. There is, however, evidence for possible overconsolidation at the very base of U1395 (from 110 to 120 mbsf), with V_p values systematically higher than model predictions in this zone. Porosity measurements (Figure 3) confirm that unexpectedly low porosities exist in this depth interval. These porosity changes, however, are accounted for in the rock physics model. The fact that V_s model results accurately replicate observations implies that V_s values are perhaps a more accurate tool for assessing velocity and pore pressure, as suggested in previous studies [*Hornbach and Manga*, 2014].

5.3. The Cause of Anomalously High Model Velocities at Site U1399

Modeled velocities at site U1399 poorly match observed in situ velocities at several depth intervals. In particular, modeled V_s velocities at site U1399 systematically overpredict measured in situ velocities at several sand-rich depth intervals at site U1399 (Figure 6). Elevated fluid pressure in some sediment at site U1399 provides the most reasonable explanation for the velocity discrepancies. We cannot easily explain the discrepancy between modeled and measured in situ velocities at site U1399 with other mechanisms. The minimum end-member velocity model already uses the theoretical minimum limit for the number of grain contacts and end-member values for mineralogy based on core analysis. We also use porosity values that are 4.5% larger than the values measured shipboard at the site. It is unlikely that in situ porosity values are higher than measured shipboard porosity, since sediment cores tend to expand during retrieval and core recovery due to depressurization, thereby increasing porosity. As a result, typical shipboard porosity measurements, especially in clay-rich sediment, are perhaps more likely to overestimate in situ porosity as opposed to underestimate it [e.g., *Scherer*, 1987; *Hoffman and Tobin*, 2004]. Porosities could, however, be higher in situ than shipboard due to grain reorganization caused by coring-related disturbances. Our analysis indicates that porosities need to increase by 15–25% (averaging between 70 and 90% porosity) to match the most significant discrepancies between modeled V_s velocities and measured in situ V_s velocities. Such high porosities do not typically exist in sand-rich marine sediment, especially sediment buried more than 100 mbsf [*Hamilton*, 1976] where porosity of sand-rich sediments rarely exceeds 50% [*Pryor*, 1973]. In normally consolidated clay-rich marine sediments, porosities only approach 70% in the first few meters below the seafloor [*Hamilton*, 1976], and not in sediments buried more than 80 mbsf unless rapid burial and significant overpressures exist. It is, therefore, difficult to explain discrepancies between modeled and measured in situ velocity with porosity uncertainties.

Anomalously low velocities at site U1399 also cannot be easily explained as a result of poor borehole conditions. The maximum caliper width of the triple-combo caliper log is ~45 cm. Caliper measurements at site U1399 indicate that an anomalously wide (~45 cm) borehole sometimes exists in a few locations where we observe high pore pressures, implying borehole collapse at these locations. Nonetheless, at most locations where we observe high pore pressure, caliper measurements are tens of centimeters below the maximum caliper width (e.g., Figure 6). We also observe some zones of anomalously low velocity where the borehole is narrower than the drill bit (30 cm); this occurs at the two deepest zones of inferred high pore pressure at site U1399. It is therefore difficult to attribute anomalously low velocities simply to changes in borehole conditions. It is intriguing, however, that the few borehole collapses that occurred at U1399 were generally in or immediately adjacent to areas where we see evidence for high pore pressure. This is perhaps not surprising since high pore pressures can lead to failure. The observation of borehole shrinkage perhaps further supports the concept that elevated fluid pressures exist at this site, since drilling would provide a pathway for expulsion of overpressured sediments, resulting in borehole compression and collapse. Alternatively, the swelling of clay-rich sediment due to hydration of overcompacted clay could also explain the decrease in drill hole diameter with time.

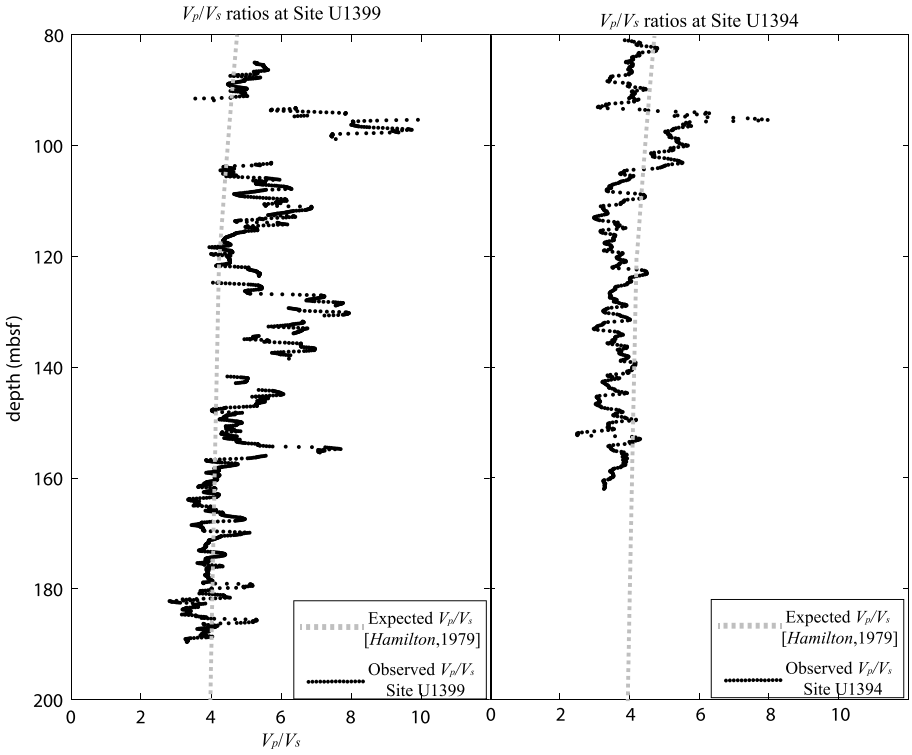

Figure 7. V_P/V_S ratios observed at sites U1399 and U1394 based on in situ wireline log measurements compared with expected values for hydrostatically pressured, normally consolidated marine sediments estimated by *Hamilton* [1979]. V_P/V_S values for normally consolidated marine sediment should generally range between 2 and 5 depending on clay and sand content [e.g., *Hamilton*, 1979; *Prasad*, 2002]. At site U1399, we observe typical (i.e., consistent with *Hamilton* [1979]) V_P/V_S values at depths greater than ~160 mbsf, as well as at ~120 mbsf and ~90 mbsf. Anomalously high V_P/V_S ratios consistent with elevated fluid pressure exist at several depth intervals at site U1399, including ~130−140 mbsf and ~90−110 mbsf. Zones where we observe anomalously high V_P/V_S ratios are consistent with depths where we infer elevated fluid pressure at site U1399 using the rock physics model. At site U1394, we observe V_P/V_S values consistent with Hamilton's predictions except between 95 and 105 mbsf, where values are anomalously high. The rock physics model predicts anomalously high fluid pressures only in this interval. The location of elevated fluid pressures at site U1394 is consistent with the predicted base of slope failure Deposit 2 (Figure 1).

With uncertainties in porosity, mineralogy, grain size, the number of grain contacts, and wireline log quality unable to explain easily the observed velocity discrepancies at site U1399, pore fluid pressure represents the last unconstrained parameter that can significantly affect seismic velocity. V_s is particularly sensitive to high pore fluid pressure. An increase in the pore fluid pressure ratio from hydrostatic to $\lambda^* = 0.7$ in sand-rich sediment will cause typical V_s values to drop by more than 20% and more than 100 m/s in sediments at site U1399. Therefore, elevated fluid pressure can in theory explain the 100–150 m/s discrepancy observed between modeled and measured in situ V_s at site U1399.

As a secondary method for assessing whether elevated fluid pressure at site U1399 might exist, we analyzed in situ V_p/V_s ratios. Typical V_p/V_s values range between 2 and 5 for normal marine sediments buried between 100 and 200 mbsf, and empirical relationships exist to predict V_p/V_s ratios with depth for normally consolidated sediment [e.g., *Hamilton*, 1979; *Han et al*., 1986; *Prasad*, 2002]. The V_p/V_s ratio is sensitive to pore pressure, with the ratio increasing exponentially as fluid pressure approaches lithostatic values [e.g., *Prasad*, 2002]. This is because as fluid pressure increases toward lithostatic values, V_p approaches water velocities (~1500 m/s), whereas V_s approaches zero. As a result, when fluid pressures increase, V_p/V_s increases, often exceeding values for normally consolidated marine sediment (between 2 and 5) [e.g., *Hamilton*, 1979; *Prasad*, 2002]. Like the rock physics approach, similar uncertainties and assumptions exist for associating V_p/V_s ratios with elevated pore pressure. Analysis of V_p/V_s using Leg 340 wireline data at site U1399 shows anomalously high V_p/V_s ratios generally exist at depths between 90 and 150 mbsf (Figure 7). These results are consistent with our rock physics model results. Finally, comparison between empirical velocity-depth

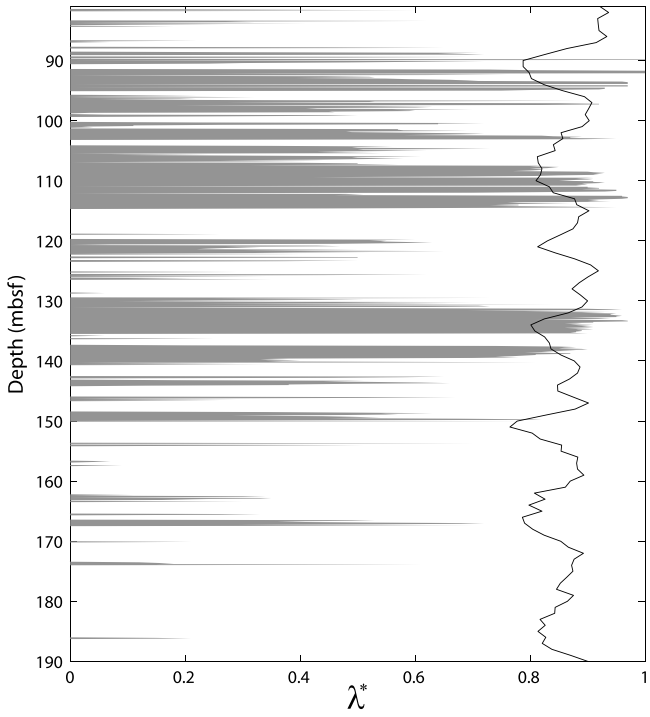

Figure 8. Pore pressure ratio λ^* versus depth at site U1399. A value of zero indicates hydrostatic fluid pressure; a value of 1 indicates lithostatic fluid pressure. Gray lines indicate model-predicted pore pressure with depth at site U1399 using the minimum end-member rock physics model to match in situ velocities. The black line indicates the minimum expected λ^* value necessary to trigger failure with depth in clay-rich sediments based on Mohr circle analysis.

profiles for normally consolidated marine sediments [e.g., *Hamilton*, 1979] with observed in situ velocity-depth profile at site U1399 also indicates that anomalously low velocities exist at site U1399 (Figure 6). This result is also consistent with elevated fluid pressures at site U1399.

5.4. Calculating the Pore Pressure Necessary to Explain Velocity Differences at U1399

A least squares analysis for data at site U1399 was conducted to determine the minimum pore pressure necessary to match rock physics modeled velocities with in situ measurements. For this analysis, we iteratively increase the pore pressure in 1% increments from hydrostatic to lithostatic values using our best estimate modeled velocity results. The analysis was conducted at ~0.1 m intervals (the resolution of the wireline data) using V_s data for the full depth range where in situ velocities exist.

The analysis suggests that fluid pressures in excess of hydrostatic values exist in much of the sediment at site U1399, with pressure at some depth intervals approaching lithostatic values (Figure 8). In general, the highest pore pressures exist at depths between ~90 and 115 mbsf and 130 and 140 mbsf where the pore pressure ratio (λ^*) averages 0.53 and 0.63, respectively. At several depths within these two intervals, the pore pressure ratio exceeds 0.8. In contrast, the pore pressure ratio outside these depth intervals averages only 0.06. Sediment with the highest fluid pressures generally correlate with sand-rich sediments where there are both incoherent seismic reflections previously associated with a large debris avalanche deposits [*Le Friant et al.*, 2004] (Figures 2b and 2c) and the highest V_p/V_s ratios.

6. Testing U1399 Results With Permeability and Consolidation Measurements

6.1. Permeability of Muds Derived From Consolidation Tests

Determining permeability and the maximum past consolidation state of sediments at site U1399 provides additional insight into sediment compaction history, fluid flow, and pore pressure. We therefore use these data to further constrain the cause of elevated fluid pressures at site U1399. Consolidation tests have been used successfully for decades to estimate sediment compaction histories and in situ pore pressures [e.g., *Moran et al.*, 1993; *Moore et al.*, 1995; *Moore and Tobin*, 1997; *Saffer*, 2003]. Consolidation tests yield the maximum past stress experienced by sediments during burial [e.g., *Casagrande*, 1936; *Becker et al.*, 1987; *Moran et al.*, 1993]. Similarly, permeability measurements provide direct insight into fluid flow rates through the sediment and therefore can be used to place first-order constraints on the sedimentation rates necessary to elevate fluid pressure [e.g., *Gibson*, 1958; *Bredehoeft and Hanshaw*, 1968].

We conducted three consolidation and permeability measurements for sediments obtained at hole U1399A using a uniaxial system in the rock physics laboratory at Penn State University. The samples consisted of three physically unaltered clay-rich cores that were 2.54 cm in diameter and 2 cm long, obtained from half-round cores at hole U1399A (Table 4). We conducted the analysis at three depths that correlate to well log depths

Table 4. Results From Permeability and Consolidation Tests at Sites U1399A and U1397B

Hole and Core Number	Depth (m) ± 2.2 mbsf	Permeability (m^2)	Pre Consolidation Stress (kPa)	Theoretical Hydrostatic Pressure (kPa)	Theoretical Effective Stress (kPa)	Overconsoidation Ratio
U1399A10H4	85	2.42×10^{-16}	1133	833	607.2	1.87
U1399A14H1	103	9.92×10^{-17}	1671	1009	742.6	2.25
U1399A17H2	133	7.52×10^{-17}	1507	1303	984.4	1.53
U1397B12H1W	92	$4.4 \pm 0.3 \times 10^{-13}$	-	-	-	-
U1397B12H2W	94	$2.8 \pm 0.2 \times 10^{-14}$	-	-	-	-

of approximately 82.9, 100.9, and 130.0 mbsf at hole U1399C. Hole U1399C was not cored and is a wireline logging hole only but is located only ~50 m from hole U1399A where there was nearly continuous core recovery to depths of approximately ~207 m [*Leg 340 Scientists*, 2012]. Correcting for depth offsets between holes U1399A and U1399C, we estimate an average standard uncertainty (1 sigma) in depth of ±2.2 m [*Leg 340 Scientists*, 2012]. We conducted consolidation and permeability measurements only on clay-rich (~ > 80% based on core description phi values) sediments at site U1399 since sand-rich sediments generally deteriorate in the uniaxial system. Permeability was measured in the vertical direction only, and σ_1 is assumed to be vertical. Significant concentrations of sand exist at several depth intervals at site U1399, particularly in areas where high pore pressures (and anomalously low velocities) exist (e.g., Figure 6), and we were unable to perform consolidation tests in these sand-rich zones.

The density of sediment at site U1399 is well constrained from drilling results, and as a result, effective (hydrostatic) vertical stress (σ_1) at site U1399 can be compared with consolidation test results to determine sediment compaction state. If stress measurements from consolidation tests match calculated effective hydrostatic stresses, we can conclude that sediments are normally consolidated. Consolidation tests yielding a maximum stress value below the expected hydrostatic effective vertical stress imply underconsolidation. Alternatively, consolidation tests yielding a maximum stress above the expected effective hydrostatic stress imply overconsolidation.

We followed the approach of *Saffer et al*. [2000] for all consolidation and permeability measurements. For initial pressure ramping, the vertical stress (σ_1) was increased at ~50 kPa/h. During this stage we also increased back pressure at similar rates to maintain low differential stress. Once σ_1 reached approximately 325 kPa and the back pressure was ~300 kPa, ~24 h lapsed to ensure that pressure was maintained and the samples were stable. We then began the final σ_1 loading phase. During final loading, σ_1 was increased by squeezing the sediment vertically at a rate of 1–3 μm/min (depending on the sample) until a clear rate change in the stress-strain relationship was observed, indicating we had exceeded the past maximum vertical stress on the sample and were now forming a virgin consolidation stress-strain curve [e.g., *Becker et al*., 1987]. During unloading, we reduced σ_1 by decompressing the sediment at a rate that ranged typically from 0.25 to 0.8 μm/min, or approximately 25% of the original σ_1 compression rate during loading.

Analysis of consolidation test results indicates that all three mud-rich hemipelagic samples at site U1399 are slightly overconsolidated, with an overconsolidation ratio averaging ~1.9 (Table 4). Measured permeability values for the three clay-rich sediment samples are 7.5×10^{-17}–2.4×10^{-16} m^2 (Table 4). These values are typical—if not slightly greater than—expected values for clay-rich sediments with 50–60% porosity such as those measured at site U1399. Permeability values for clay-rich marine sediment in this porosity range generally vary between 10^{-16} and 10^{-18} m^2 [*Neuzil*, 1994; *Gamage et al*., 2011; *Saffer et al*., 2000]. The consolidation curve and permeability for these clays indicate no evidence for overpressure in clay-rich sediment at site U1399, consistent with rock physics model results, and imply that these sediments have experienced greater strain than expected for their current burial depth.

6.2. Permeability of Sand-Rich Sediments

Unlike marine muds, sandy marine sediments should have significantly higher permeability. To better understand permeability of sand-rich sediments, we also measured the permeability of sandy turbidite deposits from site U1397B, core 12, sections 1 and 2, located just north of the submarine slide complex offshore Martinique. Measurements were made on sediment collected from the entire working half of each core section. The grain size distribution was measured on dried sediment with sieves. Because the

sediment is unconsolidated, uncemented, and noncohesive, the deposit must be recreated in the lab. Sediment was poured into a 0.1 m diameter tube and held in place by a screen of nylon fabric stretched over the bottom opening of the tube. The bottom 0.1 m of the tube was filled with sediment. A layer of sediment was adhered to the wall of the tube with a silicone sealant so that preferential flow paths did not develop along the sides of the tube. Permeability was measured using a falling-head approach with distilled water as the working fluid. Sample preparation and permeability measurements were repeated 14 times and 11 times for sediment from U1397B12H1W and U1397B12H2W, respectively. The bulk density of the water-saturated sediment was measured using the sample mass and volume and the shipboard-measured mean grain density of 2.74 g/cm^3. The mean densities for U1397B12H1W and U1397B12H2W of 1.8 and 1.6 g/cm^3, respectively, are slightly larger than but similar in magnitude to those measured on the whole round samples on the ship, 1.56 and 1.58 g/cm^3, respectively. The large size fraction in U1397B12H1W and U1397B12H2W are dominated by pumice lapilli and mud clasts, respectively. For each sediment sample, we prepared five deposits analogous to those used for the permeability measurements. Table 4 summarizes the average permeability for U1397B sediments. As might be expected, the permeability of the sand-rich sediment is 3–4 orders of magnitude greater than that measured on the hemipelagic sediment at U1399.

7. Mohr Circle Analysis

Elevated fluid pressures reduce effective stress, increasing the probability of mechanical failure. To determine if sediments at site U1399 are at or near failure, we applied Mohr circle failure criteria to sediments at site U1399. For this analysis, normal and shear stress are calculated at 1 m intervals, the maximum principle effective stress, σ_1', is vertical, and the minimum principle effective stress, σ_3', is horizontal, with each of these stresses equal to the following [*Twiss and Moores*, 1992; *Engelder and Fischer*, 1994]:

$$\sigma_1' = \rho_b g d - P_f \tag{3}$$

$$\sigma_3' = \frac{v}{1-v}\rho_b g d + \alpha\left[\frac{1-2v}{1-v}\right]P_f - P_f \tag{4}$$

where d is the depth; g is the acceleration of gravity; ρ_b is the average bulk density of sediments above (calculated directly from porosity and sediment mineralogy at site U1399); v is Poisson's ratio at each depth (calculated directly using rock physics model); α is the *Biot* coefficient of effective stress, estimated no less than 0.85 [e.g., *Lee*, 2002; *Alam et al*., 2010]; and P_f is the pore fluid pressure. Here σ_3' is a function of σ_1' and the calculation of σ_3' incorporates poroelastic effects described by *Biot* [1941] for a laterally confined basin [*Engelder and Fischer*, 1994].

We assume end-member values for the coefficient of static friction (μ_s) of 0.2–0.61, consistent with end-member clay- and sand-rich marine sediment values, respectively [*Kopf and Brown*, 2003]. We also assume sediment cohesive strength equal to ~40% of shear strength [*Ikari and Kopf*, 2011]. From these values, we calculate a minimum and maximum pore pressure ratio needed to trigger sediment failure at site U1399.

Mohr circle analysis indicates that pore pressure ratios (λ^*) as low as ~0.77 may trigger failure in clay-rich sediments with low static friction at site U1399 (Figure 8). Estimated in situ pore pressure using the rock physics models exceed a λ^* of 0.77 at several depths between 90 and 140 mbsf (Figure 8). Many of the sediments in this interval are sand rich, and likely have higher coefficients of static friction and require higher pore pressure ratios for failure. Perhaps not surprisingly, sediments at this depth interval are also the most distorted and contorted of all the sediment cores analyzed at this site [*Leg 340 Scientists*, 2012]. Our analysis therefore implies that some sediment between depths of 90 and 140 mbsf at site U1399 maintain fluid pressures that are at, or very near, the necessary pressures required for failure and, based on observed deformation at these depth intervals, have likely experienced some form of pressure-induced failure.

8. Implications for Pore Pressure Development

We use the minimum measured permeability based on consolidation tests in clay at site U1399 (7.52×10^{-17} m^2) to obtain a first-order estimate of the sedimentation rate necessary at site U1399 to explain elevated fluid pressures. Following an approach where only 1-D vertical flow, constant sedimentation, and constant permeability are assumed [*Gibson*, 1958; *Bredehoeft and Hanshaw*, 1968], our analysis indicates that

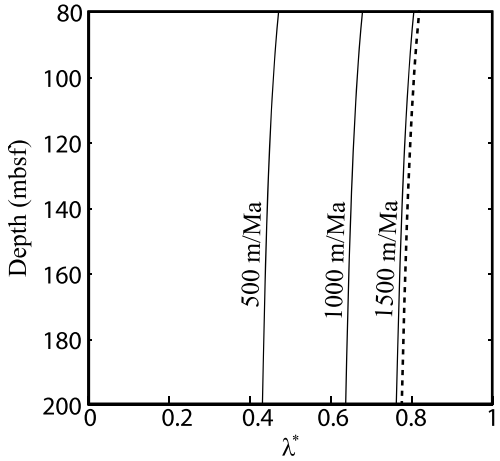

Figure 9. Pore pressure ratio for three different sedimentation rates (labeled). Results are calculated assuming constant sedimentation for 10 Ma, a constant specific storage value of 3×10^{-3} m, and a constant permeability of $7.52 \times 10^{-17} \times m^2$. The dashed black line indicates the calculated pore pressure ratio for a constant permeability value of 10^{-17} m^2 and a sedimentation rate of 200 m/Ma.

sedimentation rates of ~500–1500 m/Ma are necessary to generate λ^* values between 0.5 and 0.8 at depths between 85 and 200 mbsf (Figure 9). Note that this approach makes several assumptions, including no lateral flow. We cannot tightly constrain sedimentation rates at site U1399 using core biostratigraphy or paleomagnetic data due to significant sediment reworking [*Leg 340 Scientists*, 2012]. Sedimentation rates may be as high as 500 m/Ma in the upper few hundred meters below the seafloor [e.g., *Manga et al*., 2012]; however, most studies infer average sedimentation rates in the Grenada basin between 40 and 200 m/Ma [*Sigurdsson et al*., 1980; *Reid et al*., 1996; *Manga et al*., 2012]. It therefore appears unlikely that rapid sedimentation is the sole cause of elevated fluid pressure at site U1399 if permeability values are all generally at or above measured values. An important caveat of this analysis is that it assumes that the minimum measured permeability (7.52×10^{-17} m^2) represents the minimum permeability at site U1399. If the minimum permeability at site U1399 is lower (by less than an order of magnitude), regional sedimentation rates can in theory cause the observed elevated fluid pressures at site U1399. For example, using the same technique, a permeability of 1×10^{-17} m^2 and an average sedimentation rate of 200 m/Ma generates a pore pressure ratio as high as ~0.8 in the upper few hundred meters of sediment at site U1399 (Figure 9). Since permeability of shallowly buried clay-rich marine sediments typically range from 10^{-16} to 10^{-18} m^2 [*Neuzil*, 1994; *Gamage et al*., 2011], it is therefore plausible, and perhaps even probable, that the lowest measured permeability at site U1399 does not represent that the regional minimum and sedimentation rate alone might elevate fluid pressure at this site.

Overconsolidation of all three clay samples at site U1399 indicates either a complex burial history or complex stress history at site U1399. One possible explanation is that erosion has occurred at the site, and the sediment was previously more deeply buried, with greater vertical compaction resulting from prior greater vertical stress. Our analysis suggests that the maximum overburden stress may have been 2 times greater than it currently is today. If or how overburden was removed at site U1399 is unclear; however, all three samples suggest similar maximum past overburden values.

An alternative mechanism for sediment overcompaction that also generates overpressure is sediment deformation that more tightly organizes sediment grains while expelling fluid from pore space. This may be occurring at site U1394, with slide shearing creating a low-permeability seal that ultimately results in increased pore pressure as additional loading or shearing occurs with time (Figure 10). This mechanism may also occur at site U1399: the consolidation samples analyzed at site U1399 derive from intervals of hemipelagic mud and thin tephra layers that record evidence for deformation in the form of folding and microfaults [*Leg 340 Scientists*, 2012]. For very small shear strains, unconsolidated sediment responds elastically and there will be no change in pore pressure. However, when strains exceed ~10^{-3}, grains can rearrange and shear moduli and pore pressure will change [e.g., *Sumita and Manga*, 2008]. In contractive (high porosity) sediment, pore pressure increases during shear due to grain reorganization, and the strength can be reduced until the sediment ultimately collapses and liquefies. High pore pressure in the sands can be maintained because the low-permeability hemipelagic sediment layers bounding the sand act as confining units and allow deformation to proceed under close to undrained conditions (Figure 10e). Indeed, *Lafuerza et al*. [2014] attribute the overconsolidation at nearby site U1399, not to erosion, but to a secondary compression caused by deformation. Contractive sediment can also develop high pore pressures and liquefy owing to cyclic shear deformation, such as that produced by earthquakes. Although laboratory tests are not available to assess the loading required to reduce shear strength, *Wang and Manga* [2010], using a global compilation of observations of liquefaction, found an empirical bound on the maximum distance from an earthquake

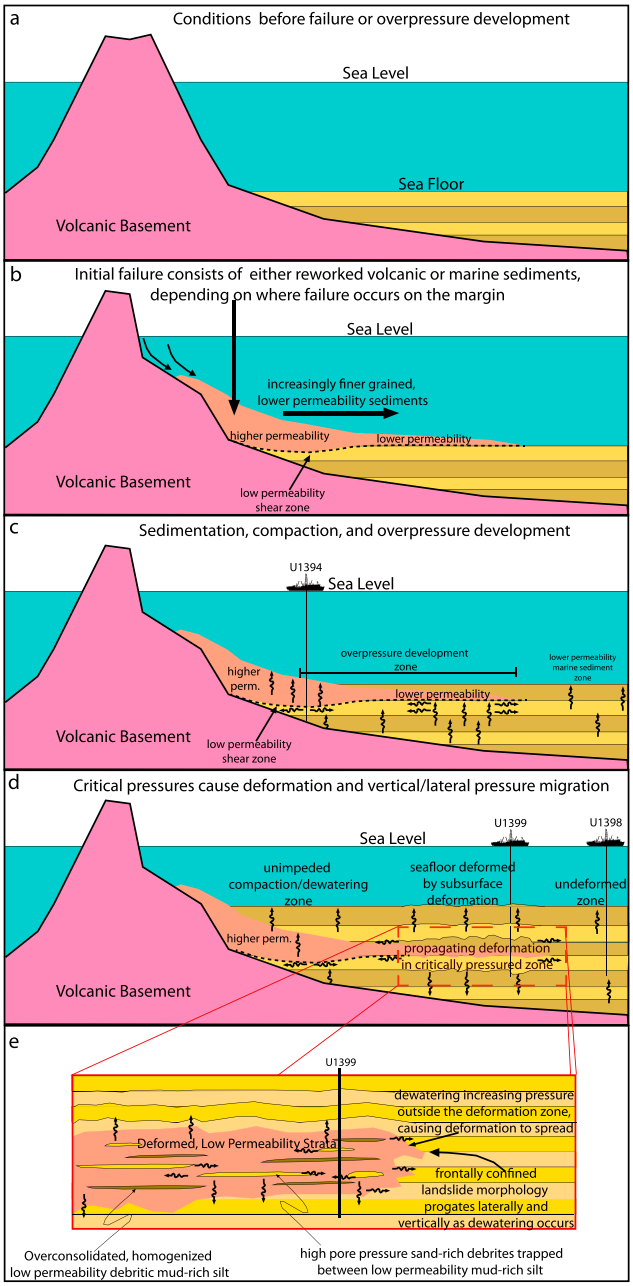

Figure 10. Schematic model for how pore pressure evolves in Lesser Antilles marine sediments. (a, b) Either marine sediment, volcanic sediment, or a combination fails along the flank of a margin. As sediments moves downslope, they naturally sort, with heavier, coarser-grained, higher-permeability sediments deposited landward and lighter, finer-grained, lower permeability sediments deposited seaward (Figure 10b). Vertical permeability will also decrease in sediments where shearing occurs along the slide base [e.g., *Yeo et al.*, 1998; *Crawford et al.*, 2008]. As a natural result of sediment shearing and sorting, (c) higher pore pressures may develop beneath lower permeability zones; high pressures immediately at the base of Deposit 2 at site U1394 may result primarily from low permeability caused by shearing at the base of the slide. (d, e) With time, additional stress changes caused by sedimentation, cyclical shearing, compaction, fluid flow, or sea level fluctuations can occur that cause pore pressures below the slide to exceed lithostatic pressure, resulting in additional failure and fluid escape. During failure, fluid must migrate out of overpressured zones, thereby reducing pressure in overpressured zones but increasing fluid pressure in adjacent sediments (Figure 10e); this increases the possibility for failure in adjacent sediments. This critical pressure scenario (Figures 10d and 10e) may be what we currently observe at site U1399. The model provides both an explanation for why many deepwater slide basal boundaries (like Deposit 1 off Martinique) are poorly defined, why deformation exists at the seafloor and appears to continue today, and why slide toes can be frontally confined, since sediments likely deform incrementally near the initial slide deposit as pressure increases and fluid escapes with time. The model therefore indicates that some of the sediment deformation we observe in seismic data (Figure 1) may postdate initial sliding and deposition.

rupture over which liquefaction might be expected in susceptible materials. For a magnitude 8 earthquake, the maximum liquefaction distance is about 400 km [*Wang et al*., 2006; *Wang and Manga*, 2010]. Earthquakes of this magnitude and within this distance occur along the Antilles subduction zone [*Bernard and Lambert*, 1988]. The maximum distance is arguably even greater for marine sediment due to evidence of greater overpressure development in fine-grained, clay-rich or gas-rich marine environments [e.g., *Day and Maslin*, 2005]. We suggest this liquefaction distance as a lower bound, since liquefaction may occur at greater distances in the marine environment. The porosity and shear strength of buried sediment are, however, likely different from surface liquefaction observations, so further analysis of sediment shear strength is needed to determine if the ~400 km distance applies to sediments in the Grenada basin.

Because the unconsolidated sands are disrupted during drilling and again during recovery, we cannot assess whether the recovered sediment is "flow liquefaction susceptible" or "cyclic mobility susceptible" [*Castro*, 1969; *Jutzeler et al*., 2014]. Consolidation tests on this material were unsuccessful because the samples fell apart during preparation or within the apparatus.

Overconsolidated clays often exist in areas prone to progressive slope failure, and several studies suggest that the geochemical and geomechanical nature of overconsolidated clays promotes failure by concentrating failure along strain-weakened slip surfaces that have reduced permeability, inhibiting compaction and pore water release [e.g., *Bjerrum*, 1967; *Palmer and Rice*, 1973]. *Stegmann et al*. [2007] used in situ measurements to demonstrate that elevated fluid pressures may exist in overconsolidated clay-rich sediments near the base of submarine slides and that many submarine landslides may therefore be triggered by pore pressure induced failure in overconsolidated sediments. It is therefore possible that the driving mechanism for slope failure at sites U1394 and U1399 is elevated fluid pressures.

An alternative to the shear hypothesis is that elevated fluid pressures develop at sites U1394 and U1399 due to differential loading and lateral fluid flow [e.g., *Dugan and Flemings*, 2000]. Specifically, if higher average sedimentation rates exist arcward, elevated fluid pressures may develop downdip from significant lateral flow in continuous, high-permeability sedimentary layers that extend from the arc into the Grenada basin. Support for this hypothesis includes the observation of high-permeability sand in the most overpressured zones at site U1399 that are bounded by lower permeability clays. This observation implies that fluid flow would be impeded less in the lateral direction and therefore preferentially flow downdip where lower initial pressures and less overburden exist. Currently, however, it is unclear if these sandy bodies consist of large, relatively continuous, hydraulically connected units that extend updip. Furthermore, temperature measurements at site U1399 and adjacent sites show no evidence for vertical advective flow [*Manga et al*., 2012].

Our analysis implies that sediment deformation could potentially result from in situ pore pressures and post-deposition grain reorganization via earthquakes (or other stress-inducing processes such as sea level change or rapid sedimentation). Since little change to the stress state is required to trigger failure at site U1399, our preferred hypothesis is that site U1399 may experience intermittent deformation as small stress changes occur at this site via compaction or ground shaking associated with regional earthquakes along the Lesser Antilles Arc, or with sea level changes associated with Pleistocene glacial cycles. Our preferred hypothesis suggests that previously interpreted slide debris at site U1399 does not actually involve large-scale sediment transport, but instead, local deformation. This hypothesis is consistent with both seismic images and core descriptions that reveal highly deformed sediment packages generally coinciding with depths where the highest fluid pressures exist in the rock physics models, but where there is little evidence for significant (kilometer-scale) downslope transport (Figure 2) [e.g., *Leg 340 Scientists*, 2012; *Le Friant et al*., 2015]. Steady, slow-slip deformation can sometimes help maintain low μ_s values, promoting further failure [*Dieterich*, 1978], although the combination of high sedimentation rates and low-permeability sediments may be the only requirement for the observed elevated fluid pressures. The landslide deposit in site U1399 is thought to be older than ~60 ka [e.g., *Boudon et al*., 2007]. Our analysis therefore implies that high excess pore pressures, perhaps maintained by lower permeability deepwater sediments, can persist subsequently for very long periods (>60 ka). We suggest that elevated pore fluid pressures exist at U1399 because sand content (and hence permeability) is generally higher in sediments at sites U1394 and U1395 [*Leg 340 Scientists*, 2012] (Figure 5 and Table 4). As a result, significantly higher sedimentation rates (>500 m/yr) or greater stress changes are likely necessary to elevated pore fluid pressure at sites U1394 and U1395 compared to U1399.

9. Additional Evidence for Slow-Slip Deformation

Analysis of pore pressure, seismic images, and seafloor bathymetry [*Boudon et al*., 2007; *Leg 340 scientists*, 2012] supports the concept that deformation at site U1399 is recent and perhaps ongoing today. Seismic images (Figures 2b and 2c) reveal a hummocky seafloor at site U1399, but a flat, undisturbed seafloor downslope, where no subsurface deformation exists. Based on the principle of original horizontality, this hummocky seafloor should not exist unless either (1) complex ocean bottom currents exist, (2) no significant sediment has been deposited since deformation occurred ~60 ka, or (3) deformation is ongoing at the site.

We suggest that deformation may be active today at site U1399 for three reasons. First, as already noted, some sediment at site U1399 has near-critical pore pressures that require minimal stress perturbations to fail. Second, multibeam images of site U1399 support the idea that seafloor hummocks imaged in seismic data near site U1399 are from recent deformation and not ocean currents [*Boudon et al*., 2007]. Third, the observations of ongoing small-scale seafloor deformation in core at site U1399 and a frontally confined slide toe in seismic data (Figure 2c) are consistent with a young, recently formed submarine landslide that is in its earliest stage of evolution due to subsurface pressure changes [e.g., *Martinsen*, 1994; *Huvenne et al*., 2002; *Frey-Martínez et al*., 2006; *Mountjoy et al*., 2009]. Specifically, we observe that as we move downslope from site U1399 toward U1398, both seafloor deformation and seismically imaged subsurface sediment deformation terminate at approximately the same seafloor location in a manner consistent with a frontally confined submarined slide (Figure 2c) [e.g., *Frey-Martínez et al*., 2006]. Our analysis therefore suggests that the slide at site U1399 is a young feature that may likely be deforming today. Additional analysis combining sediment stratigraphy with sediment age will further assess the timing and mode of deformation of these slides.

The concept of pressure-driven small-scale strain and creep-like deformation in marine sediments and submarine slides is not novel [e.g., *Mountjoy et al*., 2009]. *Lee and Chough* [2001] used their analysis of high-frequency seismic data to suggest that submarine sediments may deform in this manner and, in some instances, represent a precursor to larger-scale slope failure. Similarly, *Gardner* [2010] and *Shillington et al*. [2012] propose strain-induced pore pressures as a dominant deformation process in deepwater sediments and debris flow aprons. What is novel about results at site U1399, however, is that it quantifies for the first time pore pressure in debris flow aprons and demonstrates that near-critical overpressures do indeed sometimes exist in these environments. The analysis therefore confirms that elevated pore fluid pressure in deepwater debris flow deposits both exists and promotes deformation in these settings and may be ongoing today. We present several hypotheses to explain why elevated fluid pressure exists in these settings, but the actual cause is currently unclear and may be a combination of all the factors discussed.

10. Conclusions

Analysis of rock physics models suggests that normal (unfailed) sediments deposited at U1395 currently experience near-hydrostatic fluid pressures. In contrast, sediment at sites U1394 and U1399, where slide deposits exist, show evidence for elevated fluid pressures, with site U1394 indicating high fluid pressures at the base of the slide interface and site U1399, indicating high fluid pressures throughout the slide toe. Our analysis at site U1399 implies near-lithostatic fluid pressures in some sediment at depths between 90 and 160 mbsf. Results at U1399 generally agree with analog laboratory experiments and numerical models that infer generally lower permeability and higher sustained pore pressures in distal turbidity deposits [e.g., *Iverson*, 1997; *Lafuerza et al*., 2014]. Low permeability combined with high sedimentation rates can lead to elevated fluid pressures. However, if sedimentation rates at site U1399 range between 40 and 200 m/Ma, as some studies suggest [*Leg 340 Scientists*, 2012], we suggest that permeabilities a factor of ~7 lower than measured values at site U1399 can explain the observed pore pressure anomalies. Alternative hypotheses for elevated pore fluid pressures at site U1399 include (1) lateral fluid flow generated by differential sediment loading or (2), our preferred hypothesis, pore pressure development through regional strain and grain reorganization resulting from shear, perhaps associated with large regional earthquakes. It is well recognized that submarine slope failures often dewater sediments during transport, resulting in lower porosity and lower permeability deposits [e.g., *Sawyer et al*., 2009]. It is therefore possible that the onset of elevated fluid pressure at site U1399 began with the initial deposition, at least ~60 ka, of lower permeability slide deposits that impeded vertical flow. Subsequent pore pressure development in the region caused by periods of rapid sedimentation, earthquake-induced sediment compaction, or sea level rise would only increase fluid

pressure in the region where a low-permeability cap exists. Any additional stress at this site would act as a positive feedback mechanism for pore pressure development by further reducing the permeability of sediments during compaction while simultaneously dewatering and increasing fluid pressure, leading to further deformation with time once a critical pore pressure is reached. Thus, the low permeability of an initial slide deposit may ultimately facilitate continued deformation with time.

The technique of comparing in situ seismic velocities derived from rock physics models with in situ wireline measurements of seismic velocity provides a valuable approach for estimating in situ pore fluid pressure that is consistent with V_p/V_s analysis. These analyses are not independent as both rely on in situ V_p and V_s data. Integrating pore pressure results with Mohr circle analysis indicates that near-lithostatic fluid pressures exist in sediments deposited in the Grenada basin at site U1399 and that these sediments require minimal changes to the stress regime to fail. It implies that deepwater sediments may deform not just from an initial sliding process itself, but via post deposition stress changes. Deformed units and seismically transparent zones imaged in seismic data are often used to infer the size and shape of slope failures and associated tsunami risk [e.g., *Ward*, 2001; *Bondevik et al*., 2005; *Gee et al*., 2007]. Caution should be used interpreting the timing and size of individual slide events both in seismic data and sediment core analysis, since deformation in deepwater submarine slides may postdate sliding or initial deposition and may occur incrementally as slow-slip events. Future work integrating permeability/consolidation/velocity measurements with 2-D/3-D pore pressure models and stratigraphic interpretation of shallow sediment will provide greater insight into pore pressure evolution and sediment deformation in this region.

Acknowledgments

All data used in this study are openly available at the IODP data portal (http://www.iodp.org/access-data-and-samples) and the IODP-USIO log database maintained at Columbia University's website (http://iodp.ldeo.columbia.edu/DATA/). Additionally, all coring samples for Leg 340 are available at the IODP Texas A&M University Core Repository. This work was funded by the National Science Foundation, Integrated Ocean Drilling Program.

References

Alam, M. M., M. K. Borre, I. L. Fabricius, K. Hedegaard, B. Røgen, Z. Hossain, and A. S. Krogsbøll (2010), Biot's coefficient as an indicator of strength and porosity reduction: Calcareous sediments from Kerguelen Plateau, *J. Pet. Sci. Eng.*, *70*(3), 282–297, doi:10.1016/j.petrol.2009.11.021.

Baker, P. E. (1984), Geochemical evolution of St Kitts and Montserrat, Lesser Antilles, *J. Geol. Soc.*, *141*(3), 401–411, doi:10.1144/gsjgs.141.3.0401.

Bangs, N. L., and S. P. Gulick (2005), Physical properties along the developing décollement in the Nankai Trough: Inferences from 3-D seismic reflection data inversion and Leg 190 and 196 drilling data, in *Proceedings of the Ocean Drilling Program*, *Sci. Results*, vol. 190/196, chap. 12, pp. 1–18, Ocean Drill. Program, College Station, Tex., doi:10.2973/odp.proc.sr.190196.354.2005.

Bangs, N. L., G. K. Westbrook, J. W. Ladd, and P. Buhl (1990), Seismic velocities from the Barbados Ridge complex: Indicators of high pore fluid pressures in an accretionary complex, *J. Geophys. Res.*, *95*, 8767–8782, doi:10.1029/JB095iB06p08767.

Becker, D. E., J. H. A. Crooks, K. Been, and M. G. Jefferies (1987), Work as a criterion for determining in situ and yield stresses in clays, *Can. Geotech. J.*, *24*(4), 549–564, doi:10.1139/t87-070.

Bernard, P., and J. Lambert (1988), Subduction and seismic hazard in the northern Lesser Antilles: Revision of the historical seismicity, *Bull. Seismol. Soc. Am.*, *78*(6), 1965–1983.

Biot, M. A. (1941), General theory of three-dimensional consolidation, *J. Appl. Phys.*, *12*(2), 155–164, doi:10.1063/1.1712886.

Bjerrum, L. (1967), The Third Terzaghi Lectures: Progressive failure in slopes of overconsolidated plastic, clay and clay shales, *J. Soil Mech. Found. Div.*, *93*(5), 1–49.

Bondevik, S., F. Løvholt, C. Harbitz, J. Mangerud, A. Dawson, and J. Inge Svendsen (2005), The Storegga slide tsunami—Comparing field observations with numerical simulations, *Mar. Pet. Geol.*, *22*(1), 195–208, doi:10.1016/j.marpetgeo.2004.10.003.

Boudon, G., A. Le Friant, J. C. Komorowski, C. Deplus, and M. P. Semet (2007), Volcano flank instability in the Lesser Antilles Arc: Diversity of scale, processes, and temporal recurrence, *J. Geophys. Res.*, *112*, B08205, doi:10.1029/2006JB004674.

Bowers, G. L. (1995), Pore pressure estimation from velocity data: Accounting for overpressure mechanisms besides undercompaction, *SPE Drill. Complet.*, *10*(02), 89–95.

Boyd-Gorst, J., P. Fail, and L. Pointing (2001), 4-D time lapse reservoir monitoring of Nelson Field, Central North Sea: Successful use of an integrated rock physics model to predict and track reservoir production, *Leading Edge*, *20*(12), 1336–1350, doi:10.1190/1.1487263.

Bredehoeft, J. D., and B. B. Hanshaw (1968), On the maintenance of anomalous fluid pressures: I. Thick sedimentary sequences, *Geol. Soc. Am. Bull.*, *79*(9), 1097–1106, doi:10.1130/0016-7606.

Brown, G. M., J. G. Holland, H. Sigurdsson, J. F. Tomblin, and R. J. Arculus (1977), Geochemistry of the Lesser Antilles Island arc, *Geochim. Cosmochim. Acta*, *41*, 785–801.

Brown, K. M., D. M. Saffer, and B. A. Bekins (2001), Smectite diagenesis, pore-water freshening, and fluid flow at the toe of the Nankai wedge, *Earth Planet. Sci. Lett.*, *194*(1), 97–109.

Buatier, M. D., D. R. Peacor, and J. R. O'Neil (1992), Smectite-illite transition in Barbados accretionary wedge sediments: TEM and AEM evidence for dissolution/crystallization at low temperature, *Clays Clay Miner.*, *40*(1), 65–80.

Bugge, T., R. H. Belderson, and N. H. Kenyon (1988), The Storegga slide, *Philos. Trans. R. Soc. London A*, *325*, 357–388, doi:10.1098/rsta.1988.0055.

Burrus, J. (1998), Overpressure models for clastic rocks, their relation to hydrocarbon expulsion: A critical reevaluation, *Mem. Am. Assoc. Pet. Geol.*, 35–64.

Carstens, H., and H. Dypvik (1981), Abnormal formation pressure and shale porosity, *AAPG Bull.*, *65*(2), 344–350.

Casagrande, A. (1936), The determination of the pre-consolidation load and its practical significance, in *Proceedings of 1st International Conference on Soil Mechanics and Foundation Engineering*, vol. 3, pp. 60–64, Cambridge, Mass., A.A. Balkema, Rotterdam, Netherlands.

Cassidy, M., J. Trofimovs, M. R. Palmer, P. J. Talling, S. F. L. Watt, S. G. Moreton, and R. N. Taylor (2013), Timing and emplacement dynamics of newly recognised mass flow deposits at ~8–12 ka offshore Soufrière Hills volcano, Montserrat: How submarine stratigraphy can complement subaerial eruption histories, *J. Volcanol. Geotherm. Res.*, *253*, 1–14, doi:10.1016/j.jvolgeores.2012.12.002.

Castro, G. (1969), Liquefaction of sands, *Harvard Soil Mechanics Ser.*, *87*, Harvard Univ., Cambridge, Mass.

Cervelli, P., P. Segall, K. Johnson, M. Lisowski, and A. Miklius (2002), Sudden aseismic fault slip on the south flank of Kilauea volcano, *Nature*, *415*(6875), 1014–1018.
Crawford, B. R., D. R. Faulkner, and E. H. Rutter (2008), Strength, porosity, and permeability development during hydrostatic and shear loading of synthetic quartz-clay fault gouge, *J. Geophys. Res.*, *113*, B03207, doi:10.1029/2006JB004634.
Davis, E. E., K. Becker, T. Pettigrew, B. Carson, and R. MacDonald (1992), CORK: A hydrologic seal and downhole observatory for deep-ocean boreholes, in *Proceedings of the Ocean Drilling Program*, *Initial Rep.*, vol. 139, edited by E. E. Davis et al., pp. 43–53, Ocean Drill. Program, College Station, Tex.
Day, S., and M. Maslin (2005), Linking large impacts, gas hydrates, and carbon isotope excursions through widespread sediment liquefaction and continental slope failure: The example of the K-T boundary event, *Geol. Soc. Am. Spec. Pap.*, *384*, 239–258, doi:10.1130/0-8137-2384-1.239.
Devine, J. D. (1995), Petrogenesis of the basalt-andesite-dacite association of Grenada, Lesser Antilles island arc, revisited, *J. Volcanol. Geotherm. Res.*, *69*(1), 1–33.
Dieterich, J. H. (1978), Time-dependent friction and the mechanics of stick-slip, *Pure Appl. Geophys.*, *116*(4), 790–806, doi:10.1007/BF00876539.
Dugan, B., and P. B. Flemings (2000), Overpressure and fluid flow in the New Jersey Continental slope: Implications for slope failure and cold seeps, *Science*, *289*(5477), 288–291, doi:10.1126/science.289.5477.288.
Dutta, N. C. (2002), Geopressure prediction using seismic data: Current status and the road ahead, *Geophysics*, *67*(6), 2012–2041.
Dvorkin, J., M. Prasad, A. Sakai, and D. Lavoie (1999a), Elasticity of marine sediments: Rock physics modeling, *Geophys. Res. Lett.*, *26*, 1781–1784, doi:10.1029/1999GL900332.
Dvorkin, J., G. Mavko, and A. Nur (1999b), Overpressure detection from compressional- and shear-wave data, *Geophys. Res. Lett.*, *26*, 3417–3420, doi:10.1029/1999GL008382.
Eberhart-Phillips, D., D. H. Han, and M. D. Zoback (1989), Empirical relationships among seismic velocity, effective pressure, porosity, and clay content in sandstone, *Geophysics*, *54*(1), 82–89, doi:10.1190/1.1442580.
Eberl, D. D. (2003), User's guide to RockJock—A program for determining quantitative mineralogy from powder X-ray diffraction data, *U.S. Geol. Surv. Open-File Rep. 2003-78*, 47 pp.
Edmonds, M., and R. A. Herd (2005), Inland-directed base surge generated by the interaction of pyroclastic flows and seawater at Soufriere Hills volcano, Montserrat, *Geology*, *33*, 245–248, doi:10.1130/G21166.1.
Engelder, T., and M. P. Fischer (1994), Influence of poroelastic behavior on the magnitude of minimum horizontal stress, Sh in overpressured parts of sedimentary basins, *Geology*, *22*(10), 949–952, doi:10.1130/0091-7613(1994)022<0949:IOPBOT>2.3.CO;2.
Flemings, P. B., H. Long, B. Dugan, J. Germaine, C. M. John, J. H. Behrmann, and IODP Expedition 308 Scientists (2008), Pore pressure penetrometers document high overpressure near the seafloor where multiple submarine landslides have occurred on the continental slope, offshore Louisiana, Gulf of Mexico, *Earth Planet. Sci. Lett.*, *269*(3), 309–325, doi:10.1016/j.epsl.2007.12.005.
Frey-Martínez, J., J. Cartwright, and D. James (2006), Frontally confined versus frontally emergent submarine landslides: A 3D seismic characterisation, *Mar. Pet. Geol.*, *23*(5), 585–604.
Gamage, K., E. Screaton, B. Bekins, and I. Aiello (2011), Permeability–porosity relationships of subduction zone sediments, *Mar. Geol.*, *279*(1), 19–36, doi:10.1016/j.margeo.2010.10.010.
Gardner, J. V. (2010), The West Mariana Ridge, western Pacific Ocean: Geomorphology and processes from new multibeam data, *Geol. Soc. Am. Bull.*, *122*(9–10), 1378–1388, doi:10.1130/B30149.1.
Gassmann, F. (1951), Über die elastizität poröser medien, *Vierteljahrsschr. Naturforsch. Ges. Zuerich*, *96*, 1–23.
Gee, M. J. R., H. S. Uy, J. Warren, C. K. Morley, and J. J. Lambiase (2007), The Brunei slide: A giant submarine landslide on the North West Borneo Margin revealed by 3D seismic data, *Mar. Geol.*, *246*(1), 9–23, doi:10.1016/j.margeo.2007.07.009.
Gibson, R. E. (1958), The progress of consolidation in a clay layer increasing in thickness with time, *Geotechnique*, *8*(4), 171–182, doi:10.1680/geot.1958.8.4.171.
Hamilton, E. L. (1976), Variations of density and porosity with depth in deep-sea sediments, *J. Sediment. Petrol.*, *46*(2), 280–300.
Hamilton, E. L. (1979), V_p/V_s and Poisson's ratios in marine sediments and rocks, *J. Seismol. Soc. Am.*, *66*, 1093, doi:10.1121/1.383344.
Han, D. H., A. Nur, and D. Morgan (1986), Effects of porosity and clay content on wave velocities in sandstones, *Geophysics*, *51*(11), 2093–2107, doi:10.1190/1.1442062.
Helgerud, M. B., J. Dvorkin, A. Nur, A. Sakai, and T. Collett (1999), Elastic-wave velocity in marine sediments with gas hydrates: Effective medium modeling, *Geophys. Res. Lett.*, *26*, 2021–2024, doi:10.1029/1999GL900421.
Henriet, J.-P., A. Kano, M. J. Malone, and the Expedition 307 Project Team (2005), Modern carbonate mounds: Porcupine drilling, *IODP Sci. Prospect.*, *307*, doi:10.2204/iodp.sp.307.2005.
Hilley, G. E., R. Bürgmann, A. Ferretti, F. Novali, and F. Rocca (2004), Dynamics of slow-moving landslides from permanent scatterer analysis, *Science*, *304*(5679), 1952–1955.
Hoffman, N. W., and H. J. Tobin (2004), An empirical relationship between velocity and porosity for underthrust sediments in the Nankai Trough accretionary prisms, in *Proceedings of the Ocean Drilling Program*, *Sci. Results*, vol. 190/196, pp. 1–23, Ocean Drill. Program, College Station, Tex., doi:10.2973/odp.proc.sr.190196.355.2004.
Hornbach, M. J., and M. Manga (2014), The ability of rock physics models to infer marine in situ pore pressure, *Geochem. Geophys. Geosyst.*, *15*, 4769–4780, doi:10.1002/2014GC005442.
Hungr, O. (1995), A model for the runout analysis of rapid flow slides, debris flows, and avalanches, *Can. Geotech. J.*, *32*(4), 610–623.
Huvenne, V. A., P. F. Croker, and J. P. Henriet (2002), A refreshing 3D view of an ancient sediment collapse and slope failure, *Terra Nova*, *14*(1), 33–40.
Ikari, M. J., and A. J. Kopf (2011), Cohesive strength of clay-rich sediment, *Geophys. Res. Lett.*, *38*, L16309, doi:10.1029/2011GL047918.
Iverson, R. H. (1997), The physics of debris flows, *Rev. Geophys.*, *35*, 245–296, doi:10.1029/97RG00426.
Jutzeler, M., J. D. L. White, P. J. Talling, M. McCanta, S. Morgan, A. Le Friant, and O. Ishizuka (2014), Coring disturbances in IODP piston cores with implications for offshore record of volcanic events and the Missoula megafloods, *Geochem. Geophys. Geosyst.*, *15*, 3572–3590, doi:10.1002/2014GC005447.
Kimball, C. V., and T. L. Marzetta (1984), Semblance processing of borehole seismic array data, *Geophysics*, *49*(3), 274–281, doi:10.1190/1.1441659.
Kitajima, H., and D. M. Saffer (2012), Elevated pore pressure and anomalously low stress in regions of low frequency earthquakes along the Nankai Trough subduction megathrust, *Geophys. Res. Lett.*, *39*, L23301, doi:10.1029/2012GL053793.
Kopf, A., and K. M. Brown (2003), Friction experiments on saturated sediments and their implications for the stress state of the Nankai and Barbados subduction thrusts, *Mar. Geol.*, *202*(3), 193–210, doi:10.1016/S0025-3227(03)00286-X.
Kuenen, P. H. (1952), Estimated size of the Grand Banks [Newfoundland] turbidity current, *Am. J. Sci.*, *250*(12), 874–884.
Lafuerza, S., et al. (2014), Geomechanical characterization of submarine volcano-flank sediments, Martinique, Lesser Antilles Arc, in *Submarine Mass Movements and Their Consequences*, pp. 73–81, Springer.

Lebas, E., A. Le Friant, G. Boudon, S. F. L. Watt, P. J. Talling, N. Feuillet, C. Deplus, C. Berndt, and M. Vardy (2011), Multiple widespread landslides during the long-term evolution of a volcanic island: Insights from high-resolution seismic data, Montserrat, Lesser Antilles, *Geochem. Geophys. Geosyst.*, *12*, Q05006, doi:10.1029/2010GC003451.

Le Friant, A., G. Boudon, C. Deplus, and B. Villemant (2003a), Large-scale flank collapse events during the activity of Montagne Pelée, Martinique, Lesser Antilles, *J. Geophys. Res.*, *108*(B1), 2055, doi:10.1029/2001JB001624.

Le Friant, A., P. Heinrich, C. Deplus, and G. Boudon (2003b), Numerical simulation of the last flank-collapse event of Montagne Pelée, Martinique, Lesser Antilles, *Geophys. Res. Lett.*, *30*(2), 1034, doi:10.1029/2002GL015903.

Le Friant, A., C. L. Harford, C. Deplus, G. Boudon, R. S. J. Sparks, R. A. Herd, and J. C. Komorowski (2004), Geomorphological evolution of Montserrat (West Indies): Importance of flank collapse and erosional processes, *J. Geol. Soc.*, *161*(1), 147–160, doi:10.1144/0016-764903-017.

Le Friant, A., E. J. Lock, M. B. Hart, G. Boudon, R. S. J. Sparks, M. J. Leng, C. W. Smart, J.-C. Komorowski, C. Deplus, and J. K. Fisher (2008), Late Pleistocene tephrochronology of marine sediments adjacent to Montserrat, Lesser Antilles volcanic arc, *J. Geol. Soc.*, *165*(1), 279–289, doi:10.1144/0016-76492007-019.

Le Friant, A., C. Deplus, G. Boudon, R. S. J. Sparks, J. Trofimovs, and P. Talling (2009), Submarine deposition of volcaniclastic material from the 1995–2005 eruptions of Soufrière Hills volcano, Montserrat, *J. Geol. Soc.*, *166*(1), 171–182, doi:10.1144/0016-76492008-047.

Le Friant, A., O. Ishizuka, and N. Stroncik (2011), Lesser Antilles volcanism and landslides: Drilling volcanic landslides deposits and volcanoclastic sediments in the Lesser Antilles arc: Implications for hazard assessment and long-term magmatic evolution of the arc, *IODP Sci. Prosp.*, *340*, doi:10.2204/iodp.sp.340.2011.

Le Friant, A., et al. (2015), Submarine record of volcanic island construction and collapse in the Lesser Antilles arc: First scientific drilling of submarine volcanic island landslides by IODP Expedition 340, *Geochem. Geophys. Geosyst.*, *16*, 420–442, doi:10.1002/2014GC005652.

Lee, M. W. (2002), Biot-Gassmann theory for velocities of gas hydrate-bearing sediments, *Geophysics*, *67*(6), 1711–1719, doi:10.1190/1.1527072.

Lee, S. H., and S. K. Chough (2001), High-resolution (2–7 kHz) seismic and geometric characters of submarine creep deposits in the South Korea Plateau, East Sea, *Sedimentology*, *48*(3), 629–644, doi:10.1046/j.1365-3091.2001.00383.x.

Leg 190 Shipboard Scientific Party (2001), Leg 190 summary, in *Initial Reports of the Ocean Drilling Program*, vol. 190, pp. 1–87, Ocean Drill. Program, College Station, Tex., doi:10.2973/odp.proc.ir.190.2001.

Leg 340 Scientists (2012), *Lesser Antilles Volcanism and Landslides. Implications for Hazard Assessment and Long-Term Magmatic Evolution of the Arc, 2 March–17 April 2012*, *Integrated Ocean Drill. Program Exped. 340 Prelim. Rep.*, vol. 340, Integrated Ocean Drill. Program Manage. Int., Inc., College Station, Tex., doi:10.2204/iodp.pr.340.2012.

Lindsay, J. M., J. B. Shepherd, and D. Wilson (2005), Volcanic and scientific activity at Kick'em Jenny Submarine Volcano 2001–2002: Implications for volcanic hazard in the Southern Grenadines, Lesser Antilles, *Nat. Hazards*, *34*(1), 1–24, doi:10.1007/s11069-004-1566-2.

Liu, A. J., and S. R. Nagel (2010), The jamming transition and the marginally jammed solid, *Annu. Rev. Condens. Matter Phys.*, *1*(1), 347–369.

Macdonald, R., C. J. Hawkesworth, and E. Heath (2000), The Lesser Antilles volcanic chain: A study in arc magmatism, *Earth Sci. Rev.*, *49*(1), 1–76.

Malfait, W. J., C. Sanchez-Valle, P. Ardia, E. Médard, and P. Lerch (2011), Amorphous materials: Properties, structure, and durability compositional dependent compressibility of dissolved water in silicate glasses, *Am. Mineral.*, *96*(8), 1402–1409, doi:10.2138/am.2011.3718.

Manegold, E., and W. von Engelhardt (1933), Uber Kapillar-Systeme, XII, Die Berechnung des Stoffgehaltes heterogener Gerutstukturen, *Koll. Z.*, *63*(2), 149–154.

Manga, M., et al. (2012), Heat flow in the Lesser Antilles island arc and adjacent back arc Grenada basin, *Geochem. Geophys. Geosyst.*, *13*, Q08007, doi:10.1029/2012GC004260.

Martinsen, O. (1994), Mass movements, in *The Geological Deformation of Sediments*, pp. 127–165, Chapman and Hall, New York.

Masson, D. G., C. B. Harbitz, R. B. Wynn, G. Pedersen, and F. Løvholt (2006), Submarine landslides: Processes, triggers and hazard prediction, *Philos. Trans. R. Soc. A*, *364*(1845), 2009–2039, doi:10.1098/rsta.2006.1810.

Mattioli, G. S., et al. (2007), Unique and remarkable dilatometer measurements of pyroclastic flow-generated tsunamis, *Geology*, *35*, 25–28, doi:10.1130/G22931A.1.

Mavko, G., T. Mukerji, and J. Dvorkin (2009), *The Rock Physics Handbook: Tools for Seismic Analysis of Porous Media*, 2nd ed., pp. 1–524, Cambridge Univ. Press, New York.

Mindlin, R. D. (1949), Compliance of elastic bodies in contact, *J. Appl. Mech.*, *16*, 259–268.

Moore, J. C., and H. Tobin (1997), Estimated fluid pressures of the Barbados accretionary prism and adjacent sediments, in *Proceedings of the Ocean Drilling Program, Sci. Results*, vol. 156, pp. 229–238, Ocean Drill. Program, College Station, Tex., doi:10.2973/odp.proc.sr.156.018.1997.

Moore, J. C., et al. (1995), Abnormal fluid pressures and fault-zone dilation in the Barbados accretionary prism: Evidence from logging while drilling, *Geology*, *23*(7), 605–608, doi:10.1130/0091-7613(1995)023<0605:AFPAFZ>2.3.CO;2.

Moran, K., W. Brückmann, V. Feeser, and R. G. Campanella (1993), In situ stress conditions at Nankai trough, site 808, in *Proceeding of the Ocean Drilling Program, Sci. Results*, vol. 131, chap. 23, edited by I. A. Hill et al., pp. 28–291, Ocean Drill. Program, College Station, Tex.

Morgan, J. K., and M. V. Ask (2004), Consolidation state and strength of underthrust sediments and evolution of the décollement at the Nankai accretionary margin: Results of uniaxial reconsolidation experiments, *J. Geophys. Res.*, *109*, B03102, doi:10.1029/2002JB002335.

Mountjoy, J. J., J. McKean, P. M. Barnes, and J. R. Pettinga (2009), Terrestrial-style slow moving earthflow kinematics in a submarine landslide complex, *Mar. Geol.*, *267*(3), 114–127.

Murphy, W. F., III (1982), Effects of microstructure and pore fluids on the seismic properties of granular sedimentary materials, PhD dissertation, Stanford Univ., Stanford, Calif.

Neuzil, C. E. (1994), How permeable are clays and shales?, *Water Resour. Res.*, *30*, 145–150, doi:10.1029/93WR02930.

Owen, S., P. Segall, J. Freymueller, A. Mikijus, R. Denlinger, T. Árnadóttir, M. Sako, and R. Bürgmann (1995), Rapid deformation of the south flank of Kilauea volcano, Hawaii, *Science*, *267*(5202), 1328–1332.

Palmer, A. C., and J. R. Rice (1973), The growth of slip surfaces in the progressive failure of over-consolidated clay, *Proc. R. Soc. London A*, *332*(1591), 527–548, doi:10.1098/rspa.1973.0040.

Prasad, M. (2002), Seismic measurements in unconsolidated sands at low effective pressure and overpressure detection, *Geophysics*, *67*(2), 405–412, doi:10.1190/1.1468600.

Pryor, W. A. (1973), Permeability-porosity patterns and variations in some Holocene sand bodies, *AAPG Bull.*, *57*(1), 162–189.

Reid, R. P., S. N. Carey, and D. R. Ross (1996), Late Quaternary sedimentation in the Lesser Antilles Island arc, *Geol. Soc. Am. Bull.*, *108*, 78–100, doi:10.1130/0016-7606(1996)108<0078:LQSITL>2.3.CO;2.

Saffer, D. M. (2003), Pore pressure development and progressive dewatering in underthrust sediments at the Costa Rican subduction margin: Comparison with northern Barbados and Nankai, *J. Geophys. Res.*, *108*(B5), 2261, doi:10.1029/2002JB001787.

Saffer, D. M., E. A. Silver, A. T. Fisher, H. Tobin, and K. Moran (2000), Inferred pore pressures at the Costa Rica subduction zone: Implications for dewatering processes, *Earth Planet. Sci. Lett.*, *177*(3), 193–207.
Sawyer, D. E., P. B. Flemings, B. Dugan, and J. T. Germaine (2009), Retrogressive failures recorded in mass transport deposits in the Ursa Basin, Northern Gulf of Mexico, *J. Geophys. Res.*, *114*, B10102, doi:10.1029/2008JB006159.
Scherer, M. (1987), Parameters influencing porosity in sandstones: A model for sandstone porosity prediction, *AAPG Bull.*, *71*(5), 485–491.
Schneider, J., P. B. Flemings, B. Dugan, H. Long, and J. T. Germaine (2009), Overpressure and consolidation near the seafloor of Brazos-Trinity Basin IV, Northwest Deepwater Gulf of Mexico, *J. Geophys. Res.*, *114*, B05102, doi:10.1029/2008JB005922.
Screaton, E., D. Saffer, P. Henry, and S. Hunze (2002), Porosity loss within the underthrust sediments of the Nankai accretionary complex: Implications for overpressures, *Geology*, *30*(1), 19–22, doi:10.1130/0091-7613(2002)030<0019:PLWTUS>2.0.CO;2.
Screaton, E. J., A. T. Fisher, B. Carson, and K. Becker (1997), Barbados Ridge hydrogeologic tests: Implications for fluid migration along an active décollement, *Geology*, *25*(3), 239–242, doi:10.1130/0091-7613(1997)025<0239:BRHTIF>2.3.CO;2.
Shillington, D. J., et al. (2012), Evidence for widespread creep on the flanks of the Sea of Marmara transform basin from marine geophysical data, *Geology*, *40*(5), 439–442, doi:10.1130/G32652.1.
Sigurdsson, H., R. S. J. Sparks, C. N. Carey, and T. C. Huang (1980), Volcanogenic sedimentation in the Lesser Antilles arc, *J. Geol.*, *88*, 523–540, doi:10.1086/628542.
Smith, A. L., M. J. Roobol, and B. M. Gunn (1980), The Lesser Antilles—A discussion of the island arc magmatism, *Bull. Volcanol.*, *43*(2), 287–302, doi:10.1007/BF02598033.
Smith, W. O., P. D. Foote, and P. F. Busang (1929), Packing of homogeneous spheres, *Phys. Rev.*, *34*(9), 1271, doi:10.1103/PhysRev.34.1271.
Spinelli, G. A., P. S. Mozley, H. J. Tobin, M. B. Underwood, N. W. Hoffman, and G. W. Bellew (2007), Diagenesis, sediment strength, and pore collapse in sediment approaching the Nankai Trough subduction zone, *Geol. Soc. Am. Bull.*, *119*(3–4), 377–390, doi:10.1130/B25920.1.
Stegmann, S., H. Villinger, and A. Kopf (2006), Design of a modular, marine free-fall cone penetrometer, *Sea Technol.*, *47*(2), 27.
Stegmann, S., M. Strasser, F. Anselmetti, and A. Kopf (2007), Geotechnical in situ characterization of subaquatic slopes: The role of pore pressure transients versus frictional strength in landslide initiation, *Geophys. Res. Lett.*, *34*, L07607, doi:10.1029/2006GL029122.
Sumita, I., and M. Manga (2008), Suspension rheology under oscillatory shear and its geophysical implications, *Earth Planet. Sci. Lett.*, *269*(3), 468–477.
Tobin, H. J., and D. M. Saffer (2009), Elevated fluid pressure and extreme mechanical weakness of a plate boundary thrust, Nankai Trough subduction zone, *Geology*, *37*(8), 679–682, doi:10.1130/G25752A.1.
Trofimovs, J., R. S. J. Sparks, and P. J. Talling (2008), Anatomy of a submarine pyroclastic flow and associated turbidity current: July 2003 dome collapse event, Soufrière Hills volcano, Montserrat, West Indies, *Sedimentology*, *55*, 617–634, doi:10.1111/j.1365-3091.2007.00914.x.
Trofimovs, J., et al. (2012), Emplacement of submarine pyroclastic flows into the ocean during the 20th May 2006 dome collapse of the Soufrière Hills volcano, Montserrat, *Bull. Volcanol.*, doi:10.1007/s00445-0110533-5.
Trofimovs, J., et al. (2013), Timing, origin, and emplacement dynamics of mass flows offshore SE Montserrat in the last 110 ka: Implications for landslide and tsunami hazards, eruption history, and volcanic island evolution, *Geochem. Geophys. Geosyst.*, *14*, 385–406, doi:10.1002/ggge.20052.
Tsuji, T., H. Tokuyama, P. C. Pisani, and G. Moore (2008), Effective stress and pore pressure in the Nankai accretionary prism off the Muroto Peninsula, southwestern Japan, *J. Geophys. Res.*, *113*, B11401, doi:10.1029/2007JB005002.
Twiss, R. J., and E. M. Moores (1992), *Structural Geology*, Macmillan.
Underwood, M. B., D. M. Saffer, and A. W. McKiernan (2005), Three dimensional variations in fluid pressure and fluid production within Nankai trough subduction zone, Abstract OS24A-02 presented at 2005 Fall Meeting, AGU.
Vanorio, T., M. Prasad, and A. Nur (2003), Elastic properties of dry clay mineral aggregates, suspensions and sandstones, *Geophys. J. Int.*, *155*(1), 319–326, doi:10.1046/j.1365-246X.2003.02046.x.
Wadge, G. (1984), Comparison of volcanic production rates and subduction rates in the Lesser Antilles and Central America, *Geology*, *12*(9), 555–558, doi:10.1130/0091-7613(1984)12<555:COVPRA>2.0.CO;2.
Wang, C. Y., and M. Manga (2010), Hydrologic responses to earthquakes and a general metric, *Geofluids*, *10*(1–2), 206–216.
Wang, C. Y., A. Wong, D. S. Dreger, and M. Manga (2006), Liquefaction limit during earthquakes and underground explosions: Implications on ground-motion attenuation, *Bull. Seismol. Soc. Am.*, *96*(1), 355–363.
Ward, S. N. (2001), Landslide tsunami, *J. Geophys. Res.*, *106*, 11,201–11,215, doi:10.1029/2000JB900450.
Watt, S. F. L., et al. (2012), Widespread and progressive seafloor-sediment failure following volcanic debris avalanche emplacement: Landslide dynamics and timing offshore Montserrat, Lesser Antilles, *Mar. Geol.*, *323*(325), 69–94, doi:10.1016/j.margeo.2012.08.002.
Watt, S. F. L., P. J. Talling, and J. E. Hunt (2014), New insights into the emplacement dynamics of volcanic-island landslides, *Oceanography*, *27*, 46–57, doi:10.5670/oceanog.2014.39.
Yeo, I. W., M. H. De Freitas, and R. W. Zimmerman (1998), Effect of shear displacement on the aperture and permeability of a rock fracture, *Int. J. Rock Mech. Min. Sci.*, *35*(8), 1051–1070.